Journal of Ambient Intelligence and Humanized Computing
https://doi.org/10.1007/s12652-018-0891-3

ORIGINAL RESEARCH

Two dimensional cuckoo search optimization algorithm based despeckling filter for the real ultrasound images

Pradeep K. Gupta[1] · Shyam Lal[2] · Mustafa Servet Kiran[3,4] · Farooq Husain[1]

Received: 19 March 2018 / Accepted: 28 May 2018

Abstract
A clinical ultrasound imaging plays a significant role in the proper diagnosis of patients because, it is a cost-effective and non-invasive technique in comparison with other methods. The speckle noise contamination caused by ultrasound images during the acquisition process degrades its visual quality, which makes the diagnosis task difficult for physicians. Hence, to improve their visual quality, despeckling filters are commonly used for processing of such images. However, several disadvantages of existing despeckling filters discourage the use of existing despeckling filters to reduce the effect of speckle noise. In this paper, two dimensional cuckoo search optimization algorithm based despeckling filter is proposed for avoiding limitations of various existing despeckling filters. Proposed despeckling filter is developed by combining fast non-local means filter and 2D finite impulse response (FIR) filter with cuckoo search optimization algorithm. In the proposed despeckling filter, the coefficients of 2D FIR filter are optimized by using the cuckoo search optimization algorithm. The quantitative results comparison between the proposed despeckling filter and other existing despeckling filters are analyzed by evaluating PSNR, MSE, MAE, and SSIM values for different real ultrasound images. Results reveal that the visual quality obtained by the proposed despeckling filter is better than other existing despeckling filters. The numerical results also reveal that the proposed despeckling filter is highly effective for despeckling the clinical ultrasound images.

Keywords Optimization algorithm · Despeckling · Ultrasound image · Cuckoo search optimization algorithm

1 Introduction

Currently, in the medical field, there are many image modalities available for the diagnosis of different diseases. Out of them, ultrasound imaging is most accessible for computer aided diagnosis of patients due to its advantages like cost effectiveness, non-invasive nature, safety and feasibility to work in real time (Dhawan 2003).But, the ultrasound images used for patient diagnosis often gets degraded by speckle noise during its acquisition process. Speckle noise is introduced because of the use of phase sensitive transducer during the procedure of obtaining the ultrasound image of an organ (Cronan 2006). The nature of speckle noise is random, but it is a granular and local correlated noise. The effect of this noise is multiplicative in nature on the original image (Loupas et al. 1989). Due to the presence of speckle noise in ultrasound images, the visual, as well as quantitative analysis of such images becomes a complicated task (Szabo 2004). Therefore, we need to devise a robust despeckling filter to suppress the effect of speckle noise present in the ultrasound image before diagnosis.

✉ Shyam Lal
shyam.mtec@gmail.com

Pradeep K. Gupta
er.pradeepgupta@gmail.com

Mustafa Servet Kiran
mustafaservetkiran@gmail.com

Farooq Husain
frooqhusain100@gmail.com

[1] Department of Electronics and Communication Engineering, Moradabad Institute of Technology, Moradabad, Uttar Pradesh 244001, India

[2] Department of Electronics and Communication Engineering, National Institute of Technology Karnataka, Surathkal, Mangaluru, Karnataka 575025, India

[3] Department of Computer Engineering, Faculty of Engineering, Konya Technical University, Konya, Turkey

[4] Department of Computer Engineering, Faculty of Engineering, Selcuk University, Konya, Turkey

Published online: 02 June 2018

Many researchers have been proposed different despeckling filters and algorithms in the last two decades. These filters try to suppress the effect of speckle noise, while preserving the useful tissues for clinical purpose. The analysis of speckle noise requires being very carefully because some tissues of the ultrasound images convey the useful medical information to the physician (Thijssen and Obsterveld 1990). Out of these despeckling filters, the adaptive filters were also widely used for the speckle noise suppression because these can be easily implemented and controlled in comparison to other filters. The conventional adaptive filters are Lee's filter (Lee 1980), Frost filter (Frost et al. 1982) and Kaun's filter (Kaun et al. 1985), which calculates the effect of speckle noise by assuming the multiplicative model for noise calculation. In these filters, Gaussian distribution was used to model the speckle noise. Inaccurate modeling of speckle noise in these filters, tend to remove important details also.

Frost et al. (1982) developed an adaptive filter by using locally estimated parameter values. This filter also strikes a sense of balance between averaging and the all-pass filter, the balance is achieved by forming an exponentially shaped filter kernel that can vary from a basic average filter to an identity filter on a point-wise with adaptive manner. Further, the response of the Frost filter varies with the variation of filter coefficients. For low coefficient of variation, the filter is more average-like, and for high coefficient of variation, the filter attempts to preserve sharp features by not averaging. This filter provided minimum MSE estimation.

Kaun et al. (1985) proposed adaptive noise smoothing filter for independent noise. This filter forms an output image by computing a linear combination of the center pixel intensity in a filter window with the average intensity of the window. Hence, this filter achieves a balance between straightforward averaging and the identity filter. This balance depends on the variation of filter coefficient inside the moving window. Achim et al. (2001) converted the conventional noise model used by many researchers into additive noise model by just taking the logarithm of the image that converts the procedure, easily adaptable to all images. After that, some researchers used partial differential equation based approach to formulating new filter techniques for reducing speckle noise (Yu and Acton 2002; Santiago and Carlos 2006; Krissian et al. 2007). Yu and Acton (2002) developed a nonlinear anisotropic diffusion technique for processing the data directly, to preserve useful information present in the image. Santiago and Carlos (2006) tried to solve the problem of estimating the coefficient of variation of both signal and noise with the help of anisotropic diffusion technique, so that accurate estimation of the statistics could be performed to reduce the speckle noise. Krissian et al. (2007) proposed OSARD filter that used a matrix anisotropic diffusion method to preserve and enhance small vessel structures of the degraded images. Coupe et al. (2009) proposed a new recovery paradigm based on patch based non-local recovery. In this technique, the non-local means (NLM) filter was used for reducing speckle noise using a Bayesian framework. It helped in smoothening homogeneous areas, preserving relevant edges. Hacini et al. (2014) proposed despeckling filter based on multiplicative regularization method. The proposed denoising process was adaptive with the shape, size, and the orientation of the degraded image.

Most of the filters focused only on the reduction of speckle noise without preserving the relevant tissue information required by physicians for proper diagnosis of the disease. To overcome the existing filters problems, Ramos-Llorden et al. (2015) proposed a novel despeckling filter, driven by a probabilistic memory paradigm. Recently, Kang et al. (2016) proposed a multistate image analysis method, wherein the noisy input image is converted into its equivalent sub-bands for extracting required clinical features. The authors also claimed that the proposed method gave better diagnosis accuracy along with the better visualization of image tissues. Researchers were also focused on hybrid approaches to take advantage of the favorable traits of different methods for denoising degraded images (Hao et al. 1994; Ogier et al. 2006; Zhang et al. 2017). An integrated approach by using wavelet transform and a trilateral filter is proposed by Zhang et al. (2017). In this approach, a trilateral filter was used with wavelet shrinkage algorithm to suppress the noise. The trilateral filter suppressed the lower frequency component of speckle noise, present in the noisy image to enhance the visual quality of an image.

Meanwhile, evolutionary and swarm intelligence based approaches were also developed by researchers for the denoising of ultrasound images contaminate with speckle noise (Soni et al. 2013; de Paiva et al. 2016; Boudjelaba et al. 2011). Researchers also developed 2D adaptive filters using optimization techniques (Mastorakis and Gonos 2003; Karaboga and Getinkaya 2006). Mastorakis and Gonos (2003) used a genetic algorithm to develop a 2D recursive filter for ultrasonic image denoising. But, this method required the prior knowledge of noise added in the image for filtering. Latifoglu (2013) used Artificial Bee Colony (ABC) optimization algorithm for optimizing 2D FIR filter coefficient for the speckle noise reduction from ultrasound images. The author claimed that the proposed technique effectively eliminated speckle noise from ultrasound images compared with other state-of-the-art despeckling techniques. Malik et al. (2016) proposed an adaptive image denoising method using cuckoo search (CS) algorithm. The idea behind this approach was to optimize the filter coefficient with the help of CS algorithm. The authors claimed the robustness of the proposed technique in denoising images corrupted with different kinds of noise, compared to other methods. Kockanata and Karaboga (2015) used 2D-ABC optimization algorithm to convert a simple filter into an adaptive filter for improving denoising accuracy of the filter. The performance of proposed algorithm was compared with 2D-LMS and 2D-NLMS adaptive filters. The results showed that the 2D-ABC adaptive filter was better in comparison to other filters tested on different image datasets.

In this paper, a 2D-CS adaptive filter combining fast Non Local Means filter and 2D FIR filter with Cuckoo Search algorithm is proposed for despeckling of ultrasound images corrupted with multiplicative speckle noise.

The primary contributions of this research paper are as follows:

- A robust despeckling filter is proposed for speckle noise reduction from real ultrasound images.
- Proposed despeckling filter is developed by combining fast non local means filter and 2D FIR filter with cuckoo search optimization algorithm.

The rest of paper is structured as follows: Sect. 2 presents problem formulation. Section 3 illustrates the proposed despeckling filter based on Cuckoo Search algorithm. Section 4 gives the overview of materials and methods used in our proposed despeckling filter. To evaluate the performance of different despeckling filters, detailed analysis of results is presented in Sect. 5 and conclusions are drawn in Sect. 6.

2 Problem formulation

There is a plethora of literature describing despeckling filters and algorithms developed to reduce the speckle noise present in the ultrasound images. A particular filter is better in comparison with other if it preserves the edges of an image together with noise suppression capability.

2.1 Speckle noise model

Mostly, denoising methods for medical images adopted additive white Gaussian noise (AWGN) model for noise estimation. But, the signal dependent nature of speckle noise urges the need for specific filters for noise suppression in the ultrasound images. These filters use a multiplicative model to cope with the speckle noise since it is best suited to describe speckle noise behavior. In this model, the effect of noise is assumed to be multiplicative, and according to this model the noisy output, $I_{noisy}(m,n)$ is described as in Eq. (1).

$$I_{noisy}(m,n) = I_{org}(m,n)N(m,n) \tag{1}$$

where $I_{org}(m,n)$ is the original image and $N(m,n)$ is the speckle noise perturbation.

2.2 Fast non-local mean filter

This section gives a brief overview of the theory and fundamental concept of non-local means (NLM) filtering. The principle of NLM is based on the block-based non-local restoration of pixel (Buades et al. 2005). In this methodology, local comparison of an image pixel is replaced by the non-local comparison of blocks of the image. This approach tries to reduce the available redundancy present in the image, which gave better results in comparison with other approaches (Kevrann and Boulanger 2006; Luong et al. 2006). NLM filter works on the patterns of pixels around a pixel (Buades et al. 2005). The NLM filter processing is a process, in which a patch around a pixel is compared with other patches of the same image. The centre pixel of the patches was replaced by averaged value depending on the quadratic pixel distance between the patches (Buades et al. 2005).

Let I be the noisy image defined as $I = (I(p_i))_{p_i \in \Omega^d}$ over a bounded $\Omega^d \subset \Re^d$ rectangle region of the image where $I(p_i) \in \Re$ is noisy pixel intensity. Taking d = 2 for 2D images, we can define $NL(I)(p_i)$ to be the restored intensity value of pixel p_i calculated by weighted average of all pixel intensity values $I(p_i) \in \Re$ in the reference image. It can be mathematically formulated as in Eq. (2):

$$NL(I)(p_i) = \sum_{p_j \in \Omega^d} w(p_i, p_j) I(p_j) \tag{2}$$

where $w(p_i, p_j)$ is adaptive and depends on the extend of similarity between the pixels. That is, the weights are decided by the local neighbourhoods (patch) centred on pixels p_i and p_j such that $w(p_i, p_j) \in [0, 1]$. Therefore, in the traditional NLM filter, it is assumed that the pixel intensity of a reference pixel is linked to the pixel intensities of its local neighbourhood. This approach is known as pixel wise approach (Buades et al. 2005). Coupe et al. (2008) proposed blockwise approaches of NLM filter which reduced the computational complexity of pixel-wise approach. The main steps used in the block-wise approach are as follows:

1. Convert the noisy image region Ω^d into overlapping blocks bl_{ij} such that $\Omega^d = \bigcup_j bl_{ij}$, with permitted overlapping supports of same intensity pixel of an image.
2. Perform pixel wise approach on each block to restored the block bl_{ij} such as

$$NL(I)(bl_{ij}) = \sum_{bl_j \in \Delta_j} w(bl_{ij}, bl_j) I(bl_j). \tag{3}$$

3. Replace the intensity of pixel p_j by taking the average of the restored value of all pixels $NL(I)(bl_{ij})$.

The block wise approach reduces the complexity of the NLM filtering. The same blockwise approach was used in fast non-local means filtering to reduce the computational complexity of operation. But to make it fast, the Principal Component Algorithm (PCA) was used to process the block-wise operation of NLM filter, and hence the name is Fast Non-Local Mean filter (FNLM). The processed image of this phase is referred as $x(m, n)$.

2.3 2D-FIR filter

Stability and the nature of phase are the two important deciding parameters of a filter for a specific application. Due to its stable and linear phase nature, FIR filters are preferred in many denoising applications. The 2D FIR digital filter is defined as in Eq. (4)

$$y(m,n) = \sum_{k=0}^{M-1}\sum_{l=0}^{N-1} b_{k,l}x(m-k, n-l) \tag{4}$$

where $x(m, n)$ represents the processed image obtained as the output of FNLM filter and $y(m, n)$ denotes the 2D-FIR filtered output. The parameter $b_{k,l}$ is the weight matrix of the filter that decides the filter coefficients of 2D-FIR filter.

The transfer function of the 2D FIR filter can be defined as in Eq. (5)

$$H(z_1, z_2) = \sum_{k=0}^{M-1}\sum_{l=0}^{N-1} b_{k,l} z_1^{-k} z_2^{-l} \tag{5}$$

where $b_{k,l}$ denotes the filter coefficients of 2D FIR filter to be optimized by Cuckoo Search algorithm during the design process of proposed despeckling filter.

2.4 Fitness criterion

The fitness function is viewed as the bottle neck of cuckoo search optimization algorithm; which computes the error quality parameter between denoised and original image. An automatic despeckling approach requires a fitness function, which is independent of the manual selection of parameters. The fitness criterion for our proposed approach is the mean square error (MSE) value computed between the denoised and original image which is depicted in Eq. (6)

$$MSE = \sum_{m=0}^{M-1}\sum_{n=0}^{N-1} (I_{denoised}(m,n) - I_{org}(m,n))^2 \tag{6}$$

where $I_{org}(m, n)$ is the original image, $I_{denoised}(m, n)$ is the denoised output image and ‘M × N’ is the dimensionality of the input image.

3 Proposed despeckling filter

This section presents detailed discussion and analysis of the proposed despeckling filter. The conceptual block diagram of proposed despeckling filter is shown in Fig. 1. The proposed despeckling filter is abbreviated as 2D CS adaptive filter (2D-CSAF). The detailed description of proposed filter is given in the further subsections.

3.1 Design of proposed despeckling filter

Preserving the edges of an image during the image denoising is a very important task. Proposed despeckling filter is designed in such a way so that it preserves the edges of image after denoising. Figure 1 shows the schematic structure of proposed despeckling filter for the elimination of speckle noise in the ultrasound images. In the block diagram, the noisy image is fed to the FNLM block for pre-processing, which is followed by a 2D-FIR filtering stage. The coefficients of the 2D-FIR filter are adaptively modified using CS algorithm by evaluating the error signal $e(m, n)$. $I_{org}(m, n)$ denotes the original ultrasound image and $I_{noisy}(m, n)$ denotes the degraded image contaminated with speckle noise, $x(m, n)$ denotes the output of FNLM filter and $I_{denoised}(m, n)$ specifies the denoised image.

Yang and Deb developed a meta-heuristic optimization algorithm called Cuckoo Search algorithm, inspired by the

Fig. 1 The block diagram of the proposed despeckling filter

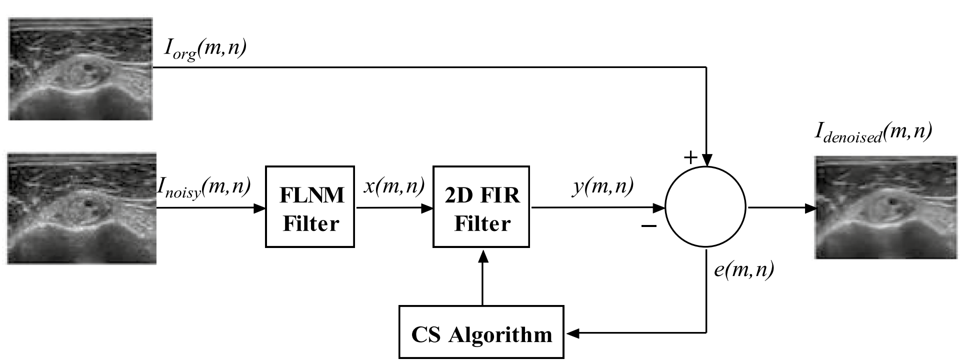

brood parasitic behavior shown by certain cuckoo species (Yang and Deb 2009; Suresh and Lal 2016). Extensive analytical studies of CS algorithm carried out by researchers have already proved its improved performance in different optimization domains (Rakhshani and Rahati 2016). One major advantage of CS algorithm as compared with others is the use of less number of parameters to optimize the solution. These reasons motivated the use of CS algorithm in the proposed despeckling filter. CS algorithm followed three major steps in its run, mimicking the hostile reproduction strategy of cuckoos in nature to increase the chances of their eggs getting hatched. The following three steps are summarized below.

1. Cuckoos lay their egg in a randomly selected host bird's nest one at a time.
2. The nest which produces the best eggs, are carried to the next generation.
3. The total number of host nests remains constant, and the probability of discovering cuckoo's egg by the host bird lies in the probability range ($p_{bn} \in [0\ 1]$).

The flow chart of the proposed despeckling filter is shown in Fig. 2 and the detailed steps and procedures included in the proposed despeckling filter are discussed below.

Step 1: The reference image $x(m, n)$ for the CS algorithm is obtained by passing $I_{noisy}(m, n)$ through two dimensional fast non-local means (2D FNLM) filter in our proposed despeckling filter.

Step 2: Initialize the population size for the weight matrix of 2D FIR Digital filter ($b_{k,l}$): $k = 1, \dots P_N; l = 1, 2 \dots p$ (P_N: no. of nests/population size), ($p = c^2$: no. of coefficient of 2D FIR filter used in the proposed scheme to form the weight matrix):

$$b_{k,l} = b_{k,l}^{min} + rand(0,1)(b_{k,l}^{max} - b_{k,l}^{min}). \tag{7}$$

Step 3: Convert the FIR filter weight matrix into 2D lexicographic form as given Eq. (8)

$$\left[b_{k,1}, b_{k,2} \dots b_{k,n+1} \dots b_{k,c}\right] \Leftrightarrow \begin{bmatrix} b_{k,1} & \dots & b_{k,n} \\ \dots & \dots & \dots \\ b_{k,n(n-1)+1} & \dots & b_{k,c} \end{bmatrix}. \tag{8}$$

Step 4: Calculate the output image estimate using the 2D filter coefficient calculation as per the Eq. (4).

Step 5: Compute the fitness value (f_t) of each possible solution using the objective function (f_{obj}) = MSE define in Eq. (6).

Repeat if no. of iteration $N_t < N_{tmax}$.

Step 6: Retain the best solution till now and generate new random solutions for the other nests in the population.

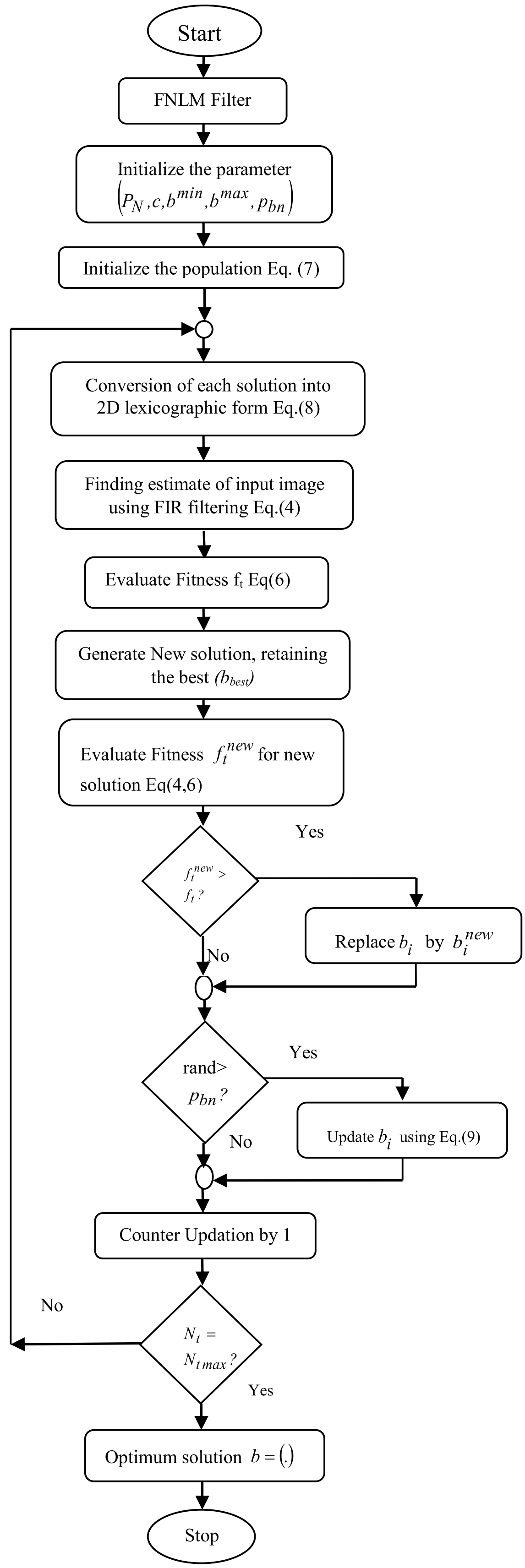

Fig. 2 Flow chart of proposed despeckling filter

Step 7: Again calculate the fitness value (f_t) for new random solution using the objective function (f_{obj}) = MSE define in Eq. (6).

Step 8: For each iteration, the probability p_{bn} altered the solution space and it is modeled as *Levy* flight Eq. (9)

$$b_i(N_t + 1) = b_i(N_t) + \alpha \oplus levy(\beta) \tag{9}$$

where α is the step size of random walks and the step size follow levy distribution (Yang and Deb 2009) give as

$$levy(\beta) = t^{-\lambda}; \quad 1 \le \lambda \le 3. \tag{10}$$

Step 9: Memorize the best solutions till now.

Step 10: Increment the iteration value N_t by 1: $N_t = N_t + 1$; until $N_t = N_{tmax}$.

Step 11: Determine $I_{denoised}(m, n)$ produced by proposed algorithm as the best solutions of the $I_{noisy}(m, n)$ with the help of optimal weight factor $b_{(..)}$ obtained by the proposed filter algorithm (2D-CSAF).

4 Materials and methods

The despeckling filters and algorithms used for experimental results comparison are: F-1: Lee filter (Lee 1980), F-2: Frost filter (Frost et al. 1982), F-3: SRAD filter (Yu and Acton 2002), F-4: DPAD filter (Santiago and Carlos 2006), F-5: Wiener filter (Hillery and Chin 1991), F-6: least mean square filter (Li et al. 2008), F-7: non local means filter (Buades et al. 2005), F-8: OBNLM filter (Coupe et al. 2009), F-9: Sig-Shrink filter (Atto et al. 2009), F-10: anisotropic diffusion filter (Ramos-Llorden et al. 2015). In addition to these filters, recent filtering algorithms such as F-11: 2D-Artificial Bee Colony (ABC) algorithm (Latifoglu 2013), F-12: 2D-ABC adaptive filtering algorithm (Kockanata and Karaboga 2015) and F-13: the proposed despeckling filter (2D-CSAF) is also considered for results comparison.

4.1 Image database

The performance comparisons of different despeckling filters and algorithms are evaluated by conducting simulation experiments on real clinical ultrasound images of shoulder rupture, thyroid gland, gall bladder, salivary gland, kidney and liver are acquired from open source medical image databases (http://www.ultrasoundcases.info and https://www.medison.ru/ultrasound).

4.2 Quality matrices

The following quality metrics were used to assess the performance of the compared filters and algorithms objectively for despeckling ultrasound images.

4.2.1 Peak signal to noise ratio (PSNR)

It is the ratio of the maximum power of a signal to the power of noise that affects the signal representations.

$$PSNR\ (\text{dB}) = 10\log_{10}\left(\frac{I_{MAX}^2}{MSE}\right) \tag{11}$$

where I_{MAX} is the maximum intensity value of input image $I(m, n)$ and MSE (mean square error) is defined as

$$MSE = \frac{1}{MN}\sum_{m=0}^{M-1}\sum_{n=0}^{N-1}\left(I_{denoised}(m,n) - I_{org}(m,n)\right)^2 \tag{12}$$

where $I_{denoised}(m, n)$ and $I_{org}(m, n)$ are the denoised and original image respectively, of dimension MxN. Higher the PSNR value, the better will be the noise suppression capability of the method whereas lower the value of MSE interpreted the better filter.

4.2.2 Mean absolute error (MAE)

It measures the degree of difference between the original image and denoised image obtained by a technique

$$MAE = \frac{1}{MN}\sum_{M=0}^{M-1}\sum_{N=0}^{N-1}\left\|I_{denoised}(m,n) - I_{org}(m,n)\right\|. \tag{13}$$

Lower the value of MAE indicates the better denoising capability of a technique.

4.2.3 Structural similarity index metric (SSIM)

The degree of similarity between the original and denoised image is measured by the parameter SSIM, and is mathematically formulated as given in Eq. (14) (Zhou et al. 2004).

$$SSIM(I, O) = \frac{(2\mu_I\mu_O + c_1)(2\sigma_{I,O} + c_2)}{(\mu_I^2 + \mu_O^2 + c_1)(\sigma_I^2 + \sigma_O^2 + c_2)} \tag{14}$$

where (μ_I, σ_I^2) and (μ_O, σ_O^2) denotes the mean and variance measures of the input and output images respectively. $\sigma_{I,O}$ denotes the covariance measured between the input and output images and constants (c_1, c_2) are used as equation stabilization factors. SSIM value varies in the range (0, 1) and a higher value of SSIM index indicates better quality of the processed image.

5 Results and discussion

In this section, we have compared the visual and quantitative performance of proposed despeckling filter with other existing despeckling filters and algorithms mentioned in Sect. 4. Simulation experiments performed on different real clinical ultrasound images. The experimental results show that the performances of the proposed despeckling filter outperformed in comparison to other existing despeckling filters and algorithms, both qualitatively and quantitatively. The proposed filter also preserves the relevant edge information of the image. The numerical values for different parameters used by other compared filters and algorithms were chosen as suggested by authors in the respective literature. All these despeckling filters and algorithms were coded using MATLAB R2015 running on intel® Core™ i3 processor with 2.53 GHz CPU, 6 GB RAM and 32-bit Windows 7 operating system.

5.1 Experimental results

The simulation experiment was conducted on ten different real clinical ultrasound images of thyroid gland, shoulder rupture, gall bladder, salivary gland, kidney and liver. To show the capability of proposed filter to remove speckle noise, different noise intensities controlled by their variance values were added to the images. The quantitative analysis results of the different despeckling filters and algorithms are presented in Tables 1, 2, 3, 4, 5, 6, 7, 8, 9 and 10 and the denoised images obtained using different filters and algorithms are shown in Fig. 3, 4, 5, 6, 7, 8, 9, 10, 11, 12, 13, 14, 15, 16, 17, 18, 19, 20, 21 and 22.

Table 1 Performance comparison of different despeckling filters for the real ultrasound image of shoulder rupture

Filter	σ = 0.10				σ = 0.20			
	PSNR	MSE	MAE	SSIM	PSNR	MSE	MAE	SSIM
F-1	20.24702	614.29701	16.40687	0.44024	19.99411	651.13268	16.58430	0.44031
F-2	22.76329	344.15321	10.14157	0.76988	22.56777	360.00092	10.24444	0.76962
F-3	22.31740	381.36462	10.62524	0.72570	22.45583	369.40056	10.79559	0.71036
F-4	10.19576	6215.90838	62.75721	0.01772	10.18455	6231.96303	62.75805	0.01778
F-5	21.15111	498.84877	14.93499	0.51745	20.59700	566.73603	15.35369	0.51810
F-6	16.14691	1579.02748	20.40093	0.44198	15.08511	2016.36425	21.83578	0.37821
F-7	25.28412	192.60552	10.05679	0.63056	24.96214	207.42738	10.31297	0.62992
F-8	26.77034	136.78763	8.46458	0.70086	26.35507	150.51287	8.78165	0.69803
F-9	29.43274	58.85815	5.34556	0.89359	24.46219	232.73489	10.65884	0.71962
F-10	23.21449	310.19243	5.89089	0.87212	22.95844	329.03044	8.04473	0.80625
F-11	19.02311	814.27089	8.79849	0.88355	19.29386	765.05882	9.41757	0.84033
F-12	28.87543	84.24377	5.67826	0.90899	25.63549	177.63629	8.86247	0.80993
F-13	30.87125	53.20533	4.94966	0.91941	27.53437	114.72099	7.33519	0.85719

Table 2 Performance comparison of different despeckling filters for the real ultrasound image of Salivary gland

Filter	σ = 0.10				σ = 0.20			
	PSNR	MSE	MAE	SSIM	PSNR	MSE	MAE	SSIM
F-1	20.96062	521.21711	15.93424	0.41112	20.68172	555.78659	16.16719	0.41149
F-2	22.23644	388.54059	10.68145	0.74041	22.07018	403.70335	10.85090	0.74025
F-3	21.93459	416.50615	11.66964	0.65722	21.80825	428.80056	11.42696	0.68034
F-4	9.81551	6784.68197	73.00005	0.01078	9.81495	6785.55227	73.00009	0.01079
F-5	22.02024	408.37200	14.25529	0.50360	21.31124	480.79050	14.91850	0.49129
F-6	16.19281	1562.42501	22.70960	0.28270	14.98506	2063.35490	24.24462	0.22306
F-7	25.28166	192.71445	10.33231	0.59839	25.08085	201.83469	10.45651	0.60297
F-8	26.86068	133.97154	8.71471	0.66532	26.41480	148.45680	9.77200	0.66164
F-9	28.05117	64.26334	6.23864	0.85320	24.05436	255.64942	12.45517	0.62715
F-10	23.94977	261.88042	6.98098	0.87080	22.77294	343.38920	9.04740	0.80061
F-11	18.93397	831.15825	9.24291	0.87843	18.85196	847.00137	10.21344	0.73260
F-12	29.47878	73.31658	5.70873	0.85923	25.50309	183.13481	9.60514	0.75771
F-13	29.60101	71.28195	6.16864	0.88975	25.52144	182.36289	9.05200	0.82909

Table 3 Performance comparison of different despeckling filters for the real ultrasound image of thyroid gland

Filter	σ = 0.10				σ = 0.20			
	PSNR	MSE	MAE	SSIM	PSNR	MSE	MAE	SSIM
F-1	20.72909	549.75745	14.06317	0.52786	20.46747	583.89287	14.24846	0.52756
F-2	23.15148	314.72584	9.07603	0.77794	22.96853	328.26698	9.19489	0.77748
F-3	23.03588	323.21561	9.38382	0.73305	22.81004	340.46821	9.29221	0.74828
F-4	11.46858	4636.84458	51.51965	0.05137	11.46772	4637.76141	51.51986	0.05144
F-5	22.78432	342.49062	12.23815	0.59084	22.02321	408.09335	12.79705	0.58492
F-6	18.10261	1006.51387	15.61117	0.52703	17.11369	1263.8967	16.12879	0.47452
F-7	26.36888	150.03492	8.40505	0.67090	24.22767	245.64815	10.14373	0.67144
F-8	22.58361	358.69012	11.75300	0.60084	22.16846	394.67067	11.97055	0.59897
F-9	28.77180	86.27801	6.22631	0.86850	25.79555	171.20837	8.73827	0.74957
F-10	25.01413	204.95927	5.59184	0.83749	23.75628	273.81215	7.79466	0.72855
F-11	19.46807	734.97672	10.89642	0.85054	19.46276	735.87604	10.59336	0.78142
F-12	24.64325	223.23147	8.58580	0.83418	24.81910	214.7314	9.55062	0.78210
F-13	31.78692	43.09121	4.38252	0.90002	25.88450	167.73757	8.69745	0.79766

Table 4 Performance comparison of different despeckling filters for the real ultrasound image of gall bladder1

Filter	σ = 0.10				σ = 0.20			
	PSNR	MSE	MAE	SSIM	PSNR	MSE	MAE	SSIM
F-1	23.51208	289.64941	10.56114	0.65477	22.92621	331.48119	10.82418	0.65312
F-2	23.96708	260.83871	6.79818	0.86107	23.68416	278.39695	7.27342	0.84240
F-3	23.88261	265.96213	7.31095	0.80499	23.76725	273.12105	7.85176	0.75509
F-4	9.51678	7267.79782	73.26798	0.06761	9.51617	7268.81630	73.26801	0.06764
F-5	24.21811	246.18967	10.57921	0.63023	23.19257	311.76222	11.32483	0.61432
F-6	16.28028	1531.27353	22.02449	0.30341	15.62614	1780.19104	20.85714	0.29622
F-7	28.94874	82.83354	6.55283	0.73686	28.06292	101.57543	6.90337	0.73680
F-8	23.77548	272.60406	9.60823	0.67505	23.26034	306.93524	9.82154	0.67472
F-9	29.69579	69.74315	6.26642	0.77497	23.67596	278.92280	12.57031	0.52678
F-10	23.90715	264.46311	6.62464	0.85785	23.10809	317.88576	9.62023	0.71925
F-11	19.92444	661.66228	8.37577	0.82994	19.17006	787.18010	7.40286	0.69457
F-12	26.14707	157.89680	8.28816	0.71700	25.13244	199.45107	9.05725	0.69713
F-13	30.58025	56.89249	5.10040	0.89939	26.97796	130.40193	8.21821	0.86178

Table 5 Performance comparison of different despeckling filters for real ultrasound image of gall bladder2

Filter	σ = 0.10				σ = 0.20			
	PSNR	MSE	MAE	SSIM	PSNR	MSE	MAE	SSIM
F-1	20.94841	522.68407	13.00961	0.52257	20.92523	525.48120	13.05513	0.52083
F-2	27.94630	104.33980	5.92266	0.83988	27.87142	106.15440	5.94590	0.84039
F-3	26.63819	141.01379	6.91772	0.80779	26.62076	141.58094	6.90835	0.80696
F-4	15.57454	1801.46891	25.99731	0.25045	15.57384	1801.75944	25.99728	0.25046
F-5	23.52909	288.51696	11.50456	0.55108	23.37033	299.25904	11.61774	0.54688
F-6	20.45910	585.01925	9.18788	0.72675	18.91167	835.43632	11.08631	0.63217
F-7	25.88926	167.55386	8.12638	0.70644	25.85764	168.77828	8.12155	0.70783
F-8	23.84914	268.01969	10.31448	0.59918	23.78690	271.88845	10.35781	0.59812
F-9	31.21170	49.19379	4.03835	0.93320	28.17373	99.01636	5.64482	0.89491
F-10	25.44480	185.60949	8.09041	0.73423	23.98780	259.59745	9.69828	0.64749
F-11	28.22117	97.94084	5.49960	0.87101	28.02493	102.46768	5.56675	0.87157
F-12	28.86480	84.45023	5.36986	0.90777	28.15677	99.40389	6.05953	0.85008
F-13	35.26327	19.35323	2.32754	0.96560	29.25329	77.22382	4.69042	0.91209

Table 6 Performance comparison of different despeckling filters for real ultrasound image of kidney1

Filter	σ = 0.10				σ = 0.20			
	PSNR	MSE	MAE	SSIM	PSNR	MSE	MAE	SSIM
F-1	21.30540	481.43827	14.45743	0.42626	21.28552	483.64696	14.54343	0.42136
F-2	25.47334	184.39385	8.68906	0.74786	25.43032	186.22940	8.72395	0.74350
F-3	26.02025	162.57556	8.39273	0.76791	25.99457	163.53965	8.36618	0.77143
F-4	15.91577	1665.34249	28.89532	0.07201	15.91475	1665.73442	28.89534	0.07211
F-5	22.25973	386.46275	14.82808	0.47139	22.19009	392.70951	14.82138	0.46676
F-6	20.67191	557.04322	9.94931	0.64399	19.08839	802.12286	12.00361	0.52100
F-7	23.39713	297.41789	12.24666	0.55609	23.31215	303.29497	12.25027	0.55488
F-8	22.72284	347.37344	13.85955	0.48935	22.53433	362.78298	14.85138	0.51506
F-9	33.23794	30.85223	3.35357	0.94866	29.68393	69.93380	5.19880	0.84628
F-10	32.38285	37.56602	4.04546	0.89297	28.77160	86.28196	5.97995	0.86729
F-11	26.32074	151.70717	7.10507	0.81233	24.90887	209.98722	8.77376	0.75575
F-12	29.90557	66.45434	5.52618	0.90506	27.24670	122.57749	7.53572	0.85653
F-13	35.65739	17.67426	2.58632	0.95319	31.43821	46.69379	4.03126	0.87771

Table 7 Performance comparison of different despeckling filters for real ultrasound image of gall bladder3

Filter	σ = 0.10				σ = 0.20			
	PSNR	MSE	MAE	SSIM	PSNR	MSE	MAE	SSIM
F-1	18.34031	952.90523	19.61046	0.30712	18.29033	963.93471	19.72203	0.30405
F-2	22.32970	380.28578	12.88086	0.57417	22.30742	382.24172	12.86769	0.58137
F-3	21.94457	415.55040	13.35828	0.56395	21.78974	430.63182	13.58702	0.55895
F-4	9.31042	7621.46087	66.71809	0.14931	9.31035	7621.57781	66.71806	0.14930
F-5	20.10831	634.23428	19.02098	0.35742	19.93018	660.78775	19.35723	0.35133
F-6	13.29920	3042.00542	30.30289	0.33495	11.95154	4148.83865	36.84209	0.27535
F-7	22.52427	363.62462	13.00670	0.53612	22.42051	372.41693	13.03914	0.54425
F-8	20.22084	618.01111	17.35130	0.36509	20.15199	627.88668	17.45901	0.36347
F-9	25.03133	204.14905	9.20979	0.82812	23.26414	306.66677	11.69083	0.72559
F-10	22.06010	404.64165	13.23811	0.53716	20.92013	526.09885	15.20301	0.44408
F-11	22.39744	374.40068	13.01901	0.69838	21.49911	460.43614	13.88226	0.64230
F-12	21.44567	466.13649	14.62515	0.66259	21.74636	434.95482	14.41520	0.64911
F-13	29.21097	77.98010	5.88410	0.88931	24.21503	246.36432	10.27277	0.81105

Table 8 Performance comparison of different despeckling filters for real ultrasound image of kidney2

Filter	σ = 0.10				σ = 0.20			
	PSNR	MSE	MAE	SSIM	PSNR	MSE	MAE	SSIM
F-1	24.05742	255.46923	8.54049	0.60078	24.04259	256.34268	8.57954	0.59939
F-2	27.42490	117.64968	5.71325	0.75873	27.35378	119.59204	5.76384	0.75782
F-3	27.25339	122.38884	5.88072	0.75291	27.11563	126.33323	6.06303	0.74218
F-4	14.08886	2536.26331	35.95979	0.26470	14.08903	2536.16454	35.95979	0.26473
F-5	26.94569	131.37457	7.62585	0.64482	26.54826	143.96416	7.94236	0.62794
F-6	19.63800	706.77350	11.73814	0.51137	18.28879	964.27548	12.95507	0.46011
F-7	26.42472	148.11831	7.10169	0.65537	26.39431	149.15885	7.09722	0.65739
F-8	24.94800	208.10379	8.37597	0.58197	24.22822	245.61691	10.40627	0.59287
F-9	28.82866	85.15574	5.51156	0.83833	27.55995	114.04740	5.58113	0.73417
F-10	27.30472	120.95059	5.89069	0.73572	26.31149	152.03078	6.72296	0.67940
F-11	27.69600	110.52993	5.60669	0.78398	25.41468	186.90130	8.17276	0.68479
F-12	27.06052	127.94637	6.33070	0.78735	26.78876	136.20851	7.13199	0.69694
F-13	33.89146	26.54207	3.19496	0.88984	27.83593	107.02549	6.43667	0.79709

Table 9 Performance comparison of different despeckling filters for real ultrasound image of liver1

Filter	σ = 0.10				σ = 0.20			
	PSNR	MSE	MAE	SSIM	PSNR	MSE	MAE	SSIM
F-1	22.93930	330.48400	8.61406	0.61126	22.92451	331.61140	8.66385	0.61010
F-2	27.22166	123.28615	5.52766	0.78924	27.22340	123.23676	5.58093	0.78847
F-3	26.49390	145.77745	5.96273	0.77947	26.24144	154.50266	6.03671	0.77366
F-4	16.55267	1438.18128	25.41887	0.25734	16.55229	1438.30776	25.41888	0.25737
F-5	26.84537	134.44463	7.03062	0.67123	26.41624	148.40757	7.27331	0.66298
F-6	21.19873	493.40884	8.14248	0.63823	19.86494	670.78896	8.85450	0.57197
F-7	26.39453	149.15144	6.75652	0.68421	26.23865	154.60205	6.81113	0.68328
F-8	24.55176	227.98419	8.14642	0.61829	24.52705	229.28477	8.15657	0.61826
F-9	32.20376	39.14752	3.54353	0.92003	30.37675	59.62179	4.55900	0.82375
F-10	26.32313	151.62387	6.08885	0.76238	25.16089	198.14889	7.03154	0.70231
F-11	28.80002	85.71926	4.65902	0.86033	28.00398	102.96325	4.97978	0.83227
F-12	30.15266	62.77903	4.70781	0.89797	29.93766	65.96508	4.76849	0.84831
F-13	36.27750	15.32254	2.28854	0.94018	31.31275	48.06244	4.01117	0.91042

Table 10 Performance comparison of different despeckling filters for real ultrasound image of liver2

Filter	σ = 0.10				σ = 0.20			
	PSNR	MSE	MAE	SSIM	PSNR	MSE	MAE	SSIM
F-1	21.81625	428.01148	12.15553	0.54160	21.78166	431.43356	12.21742	0.53872
F-2	27.04536	128.39382	6.36013	0.78223	26.96858	130.68388	6.43142	0.78270
F-3	26.30419	152.28652	6.84685	0.77251	26.13154	158.46261	6.99487	0.76402
F-4	12.81487	3400.89369	40.30005	0.18707	12.81502	3400.78076	40.30028	0.18703
F-5	23.81467	270.15492	11.58896	0.58903	23.45623	293.39816	12.03357	0.56664
F-6	17.95762	1040.68168	13.73949	0.54251	16.16891	1571.04639	16.53476	0.45563
F-7	25.60638	178.83065	8.08450	0.68663	25.45258	185.27758	8.11966	0.68952
F-8	23.60903	283.25476	10.36382	0.57783	23.54310	287.58784	10.40466	0.57519
F-9	29.96527	65.54702	4.72236	0.89940	26.68444	139.52005	7.08911	0.74654
F-10	26.91067	132.43830	7.38618	0.72199	23.25471	307.33347	10.89030	0.56794
F-11	27.23544	122.89571	6.15581	0.84469	27.10323	126.69438	6.39016	0.82539
F-12	28.65463	88.63746	5.48077	0.87131	26.36081	150.31402	7.50814	0.79105
F-13	32.64624	35.35546	3.56054	0.90467	27.56046	114.03396	6.03806	0.83608

5.2 Discussions

The images used for experiments include the real clinical ultrasound images of shoulder rupture, thyroid gland, gall bladder, salivary gland, kidney and liver. We used CSA as an optimization tool in our proposed filter algorithm due to the simplicity of CSA algorithms. CSA depends only on a single control parameter p_{bn}. The parameter p_{bn} denotes the probability of discovering Cuckoo's egg by the host bird. The optimal value of p_{bn} used by 2D FIR filter weight optimization was chosen to be 0.50; the remaining parameter of the proposed 2D-CSAF algorithm P_N, c, w^{min}, w^{max} and N_{tmax} was chosen to be 30, 9, -1, 1 and 30 respectively. The different optimum values for parameters used by other compared filters were adopted as recommended by the researchers in the literature. The quality metrics compared are PSNR, MSE, MAE, and SSIM.

Figures 3 and 4 shows the visual result comparison of different despeckling filters and algorithms on the real clinical ultrasound image of rupture shoulder. Figures 5 and 6 shows the visual result comparison of different despeckling filters and algorithms on the real clinical ultrasound image of salivary gland. Figures 7 and 8 shows the visual result comparison of different despeckling filters and algorithms on the real clinical ultrasound image of thyroid gland. Figures 9 and 10 shows the visual result comparison of different despeckling filters and algorithms on the real clinical ultrasound image of gall bladder1. Figures 11 and 12 shows the visual result comparison of different despeckling filters and algorithms on the real clinical ultrasound image of gall bladder2. Figures 13 and 14 shows the visual result comparison of different despeckling filters and algorithms on the real clinical ultrasound image of kidney1. Figures 15 and 16 shows the visual result comparison of different despeckling filters and

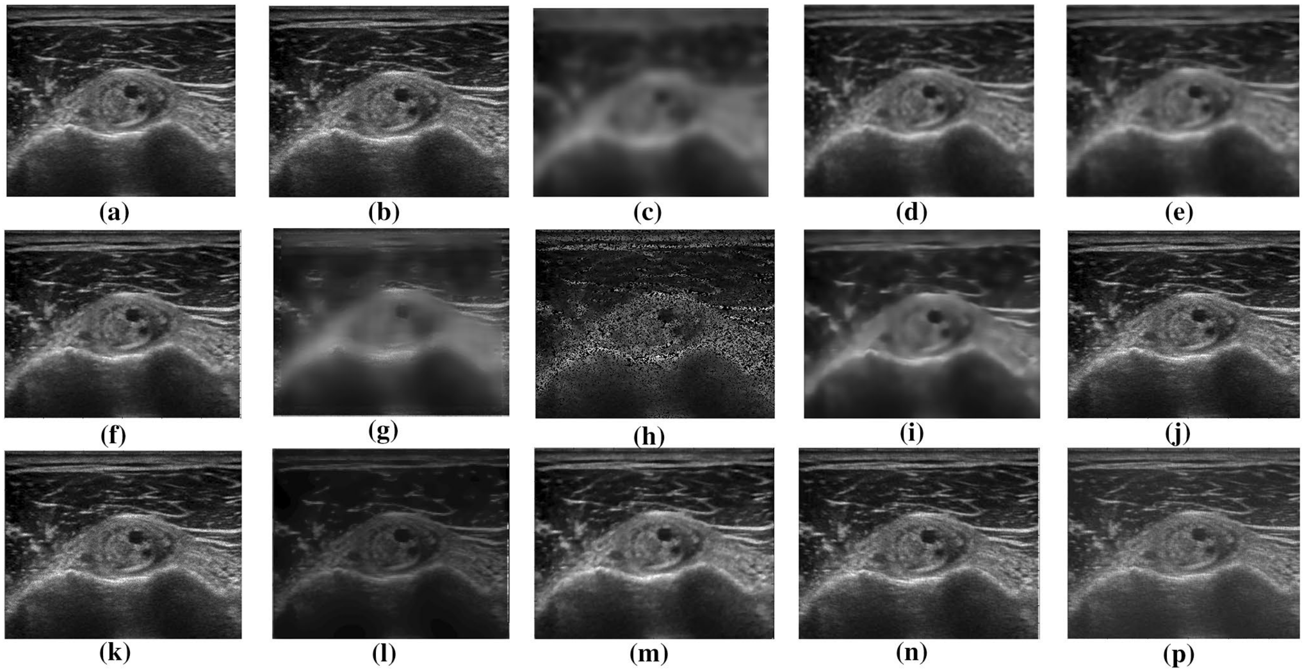

Fig. 3 Denoised image outputs using different filtering algorithms for the real ultrasound image of shoulder rupture for the value of σ = 0.10. **a** Original image, **b** noisy image, **c** F-1, **d** F-2, **e** F-3, **f** F-4, **g** F-5, **h** F-6, **i** F-7, **j** F-8, **k** F-9, **l** F-10, **m** F-11, **n** F-12, **p** F-13

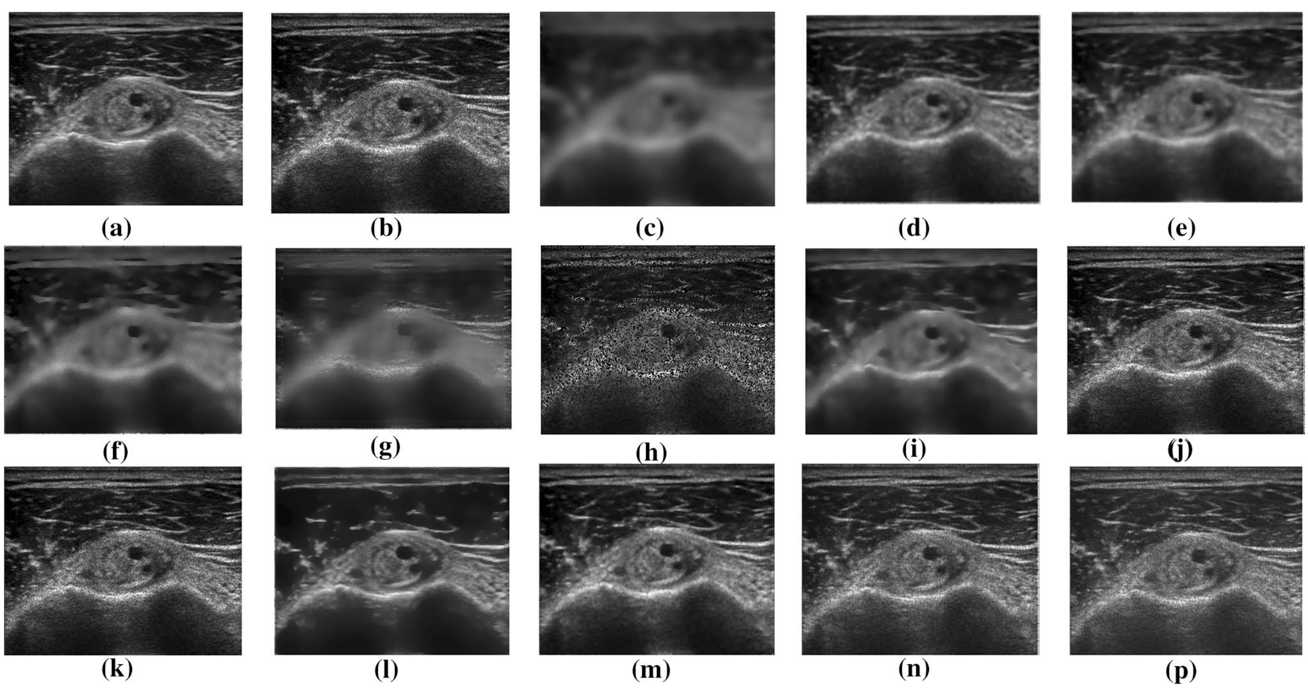

Fig. 4 Denoised image outputs using different filtering algorithms for the real ultrasound image of shoulder rupture for the value of σ = 0.20. **a** Original image, **b** noisy image, **c** F-1, **d** F-2, **e** F-3, **f** F-4, **g** F-5, **h** F-6, **i** F-7, **j** F-8, **k** F-9, **l** F-10, **m** F-11, **n** F-12, **p** F-13

algorithms on the real clinical ultrasound image of gall bladder3. Figures 17 and 18 shows the visual result comparison of different despeckling filters and algorithms on the real clinical ultrasound image of kidney2. Figures 19 and 20 shows the visual result comparison of different despeckling filters and algorithms on the real clinical ultrasound image

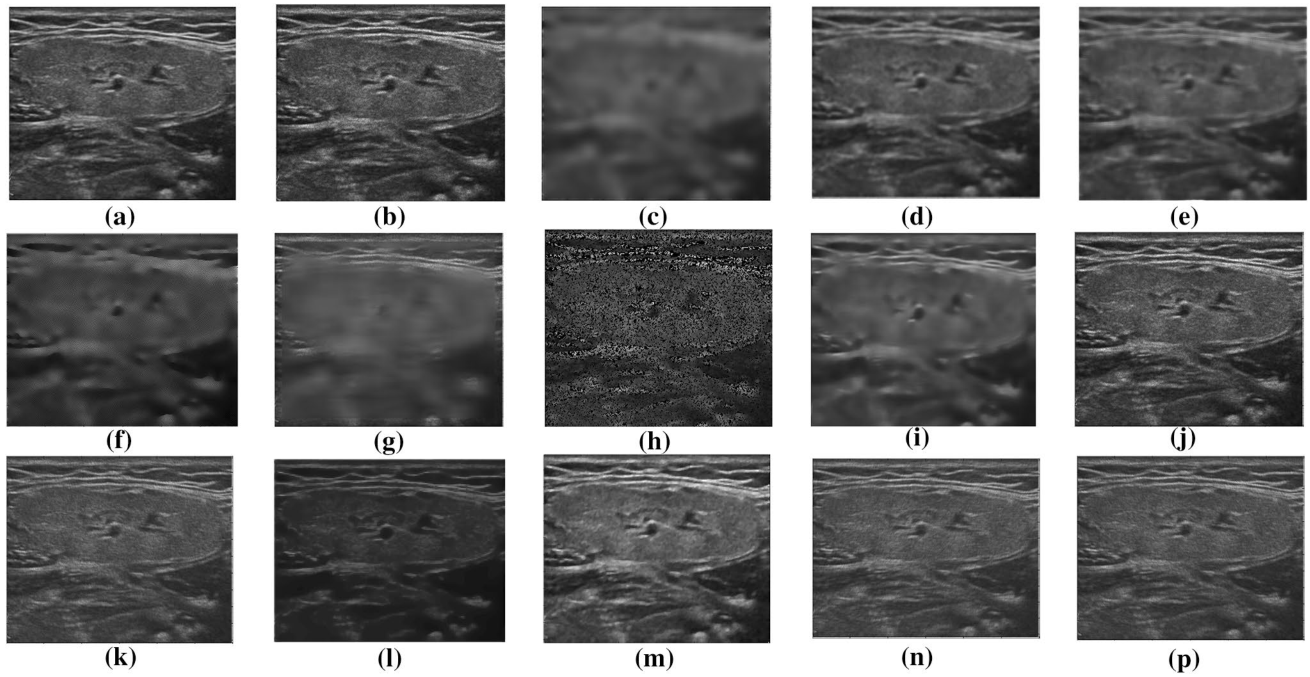

Fig. 5 Denoised image outputs using different filtering algorithms for the real ultrasound image of Salivary gland for the value of σ = 0.10. **a** Original image, **b** noisy image, **c** F-1, **d** F-2, **e** F-3, **f** F-4, **g** F-5, **h** F-6, **i** F-7, **j** F-8, **k** F-9, **l** F-10, **m** F-11, **n** F-12, **p** F-13

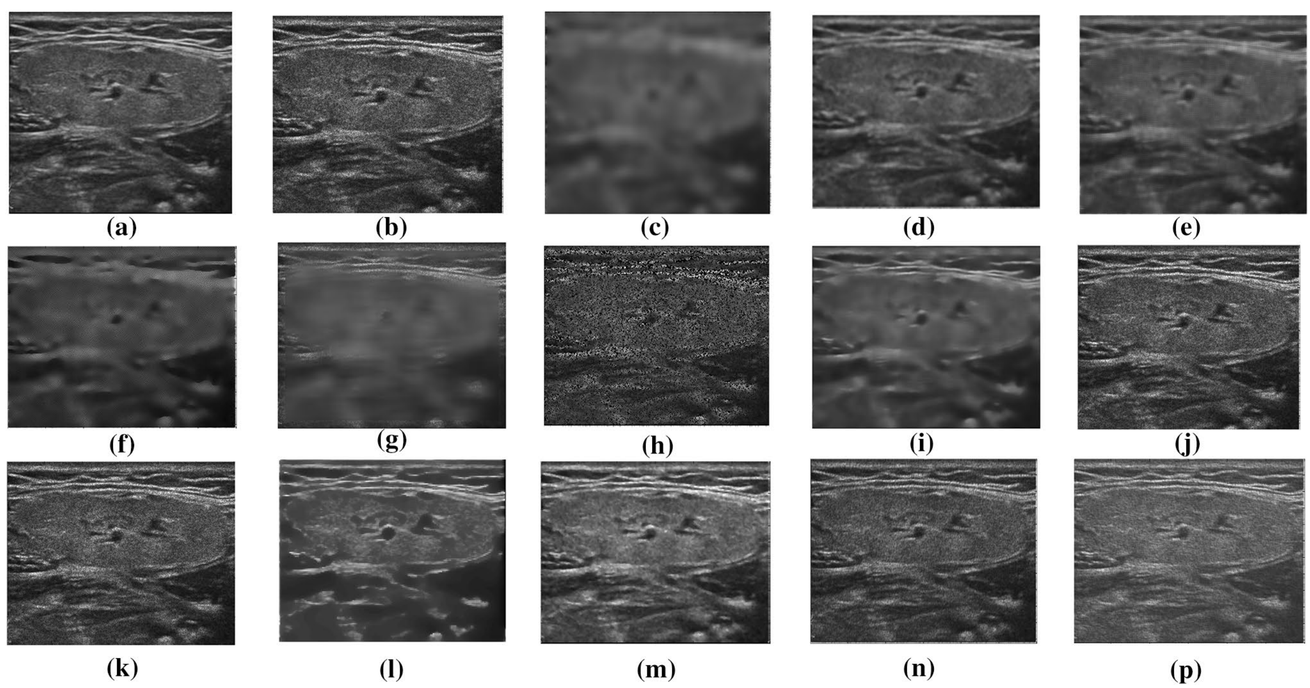

Fig. 6 Denoised image outputs using different filtering algorithms for the real ultrasound image of Salivary gland for the value of σ = 0.20. **a** Original image, **b** noisy image, **c** F-1, **d** F-2, **e** F-3, **f** F-4, **g** F-5, **h** F-6, **i** F-7, **j** F-8, **k** F-9, **l** F-10, **m** F-11, **n** F-12, **p** F-13

of liver1. Figures 21 and 22 shows the visual result comparison of different despeckling filters and algorithms on the real clinical ultrasound image of liver2, for different noise variance levels σ = 0.1 and 0.2 respectively. From the visual result comparison of all the output despeckled images, it is observed that the proposed two dimensional cuckoo search

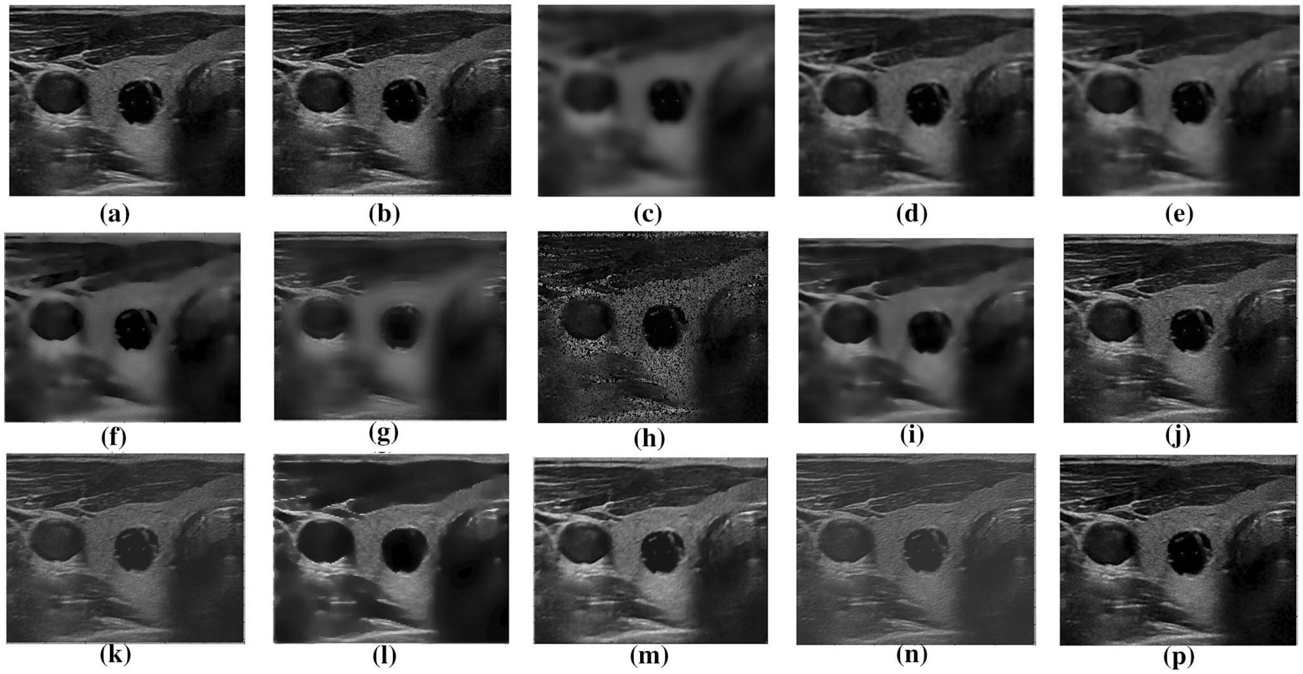

Fig. 7 Denoised image outputs using different filtering algorithms for the real ultrasound image of thyroid gland for the value of σ = 0.10. **a** Original image, **b** noisy image, **c** F-1, **d** F-2, **e** F-3, **f** F-4, **g** F-5, **h** F-6, **i** F-7, **j** F-8, **k** F-9, **l** F-10, **m** F-11, **n** F-12, **p** F-13

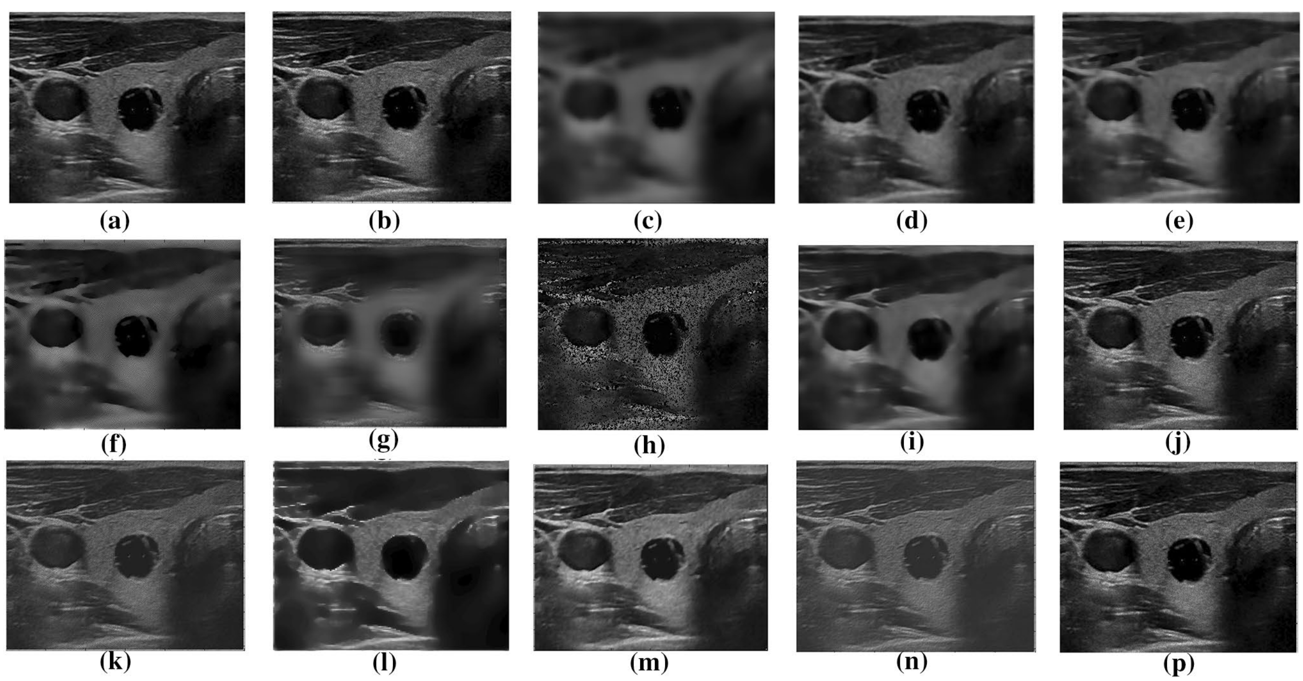

Fig. 8 Denoised image outputs using different filtering algorithms for the real ultrasound image of thyroid gland for the value of σ = 0.20. **a** Original image, **b** noisy image, **c** F-1, **d** F-2, **e** F-3, **f** F-4, **g** F-5, **h** F-6, **i** F-7, **j** F-8, **k** F-9, **l** F-10, **m** F-11, **n** F-12, **p** F-13

optimization algorithm based despeckling filter gives better results as compared to other existing despeckling filters and algorithms. It also provides better edge preservation capability, more smoother images, less blurring effect and better noise suppression capability for different noise variance levels.

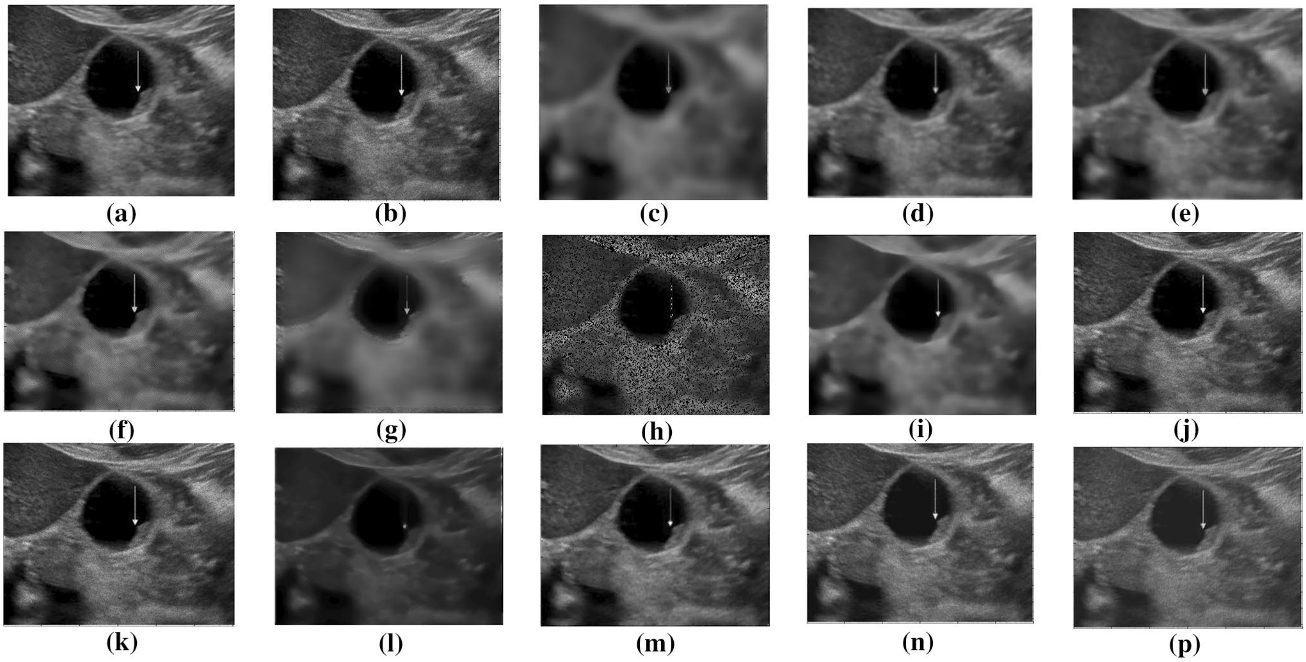

Fig. 9 Denoised image outputs using different filtering algorithms for the real ultrasound image of gall bladder1 for the value of σ = 0.10. **a** Original image, **b** noisy image, **c** F-1, **d** F-2, **e** F-3, **f** F-4, **g** F-5, **h** F-6, **i** F-7, **j** F-8, **k** F-9, **l** F-10, **m** F-11, **n** F-12, **p** F-13

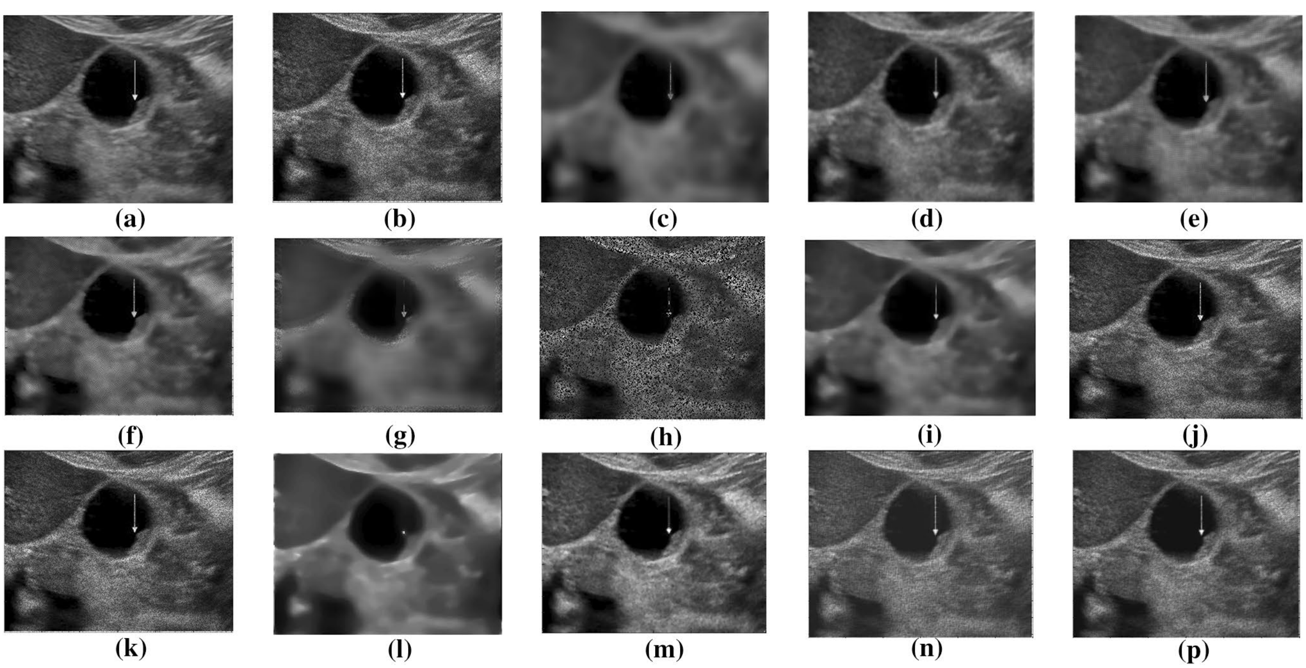

Fig. 10 Denoised image outputs using different filtering algorithms for the real ultrasound image of gall bladder1 for the value of σ = 0.20. **a** Original image, **b** noisy image, **c** F-1, **d** F-2, **e** F-3, **f** F-4, **g** F-5, **h** F-6, **i** F-7, **j** F-8, **k** F-9, **l** F-10, **m** F-11, **n** F-12, **p** F-13

The quantitative results evaluation of the proposed despeckling filter are supported by the different quality metrics are listed in Tables 1, 2, 3, 4, 5, 6, 7, 8, 9 and 10 for the real clinical ultrasound images of shoulder, salivary gland, thyroid gland, gall bladder1, gall bladder2, kidney1, gall bladder3, kidney2, liver1 and liver2 respectively for the different noise levels. We compared the speckle noise suppression capability of the proposed despeckling filter with 12 different existing

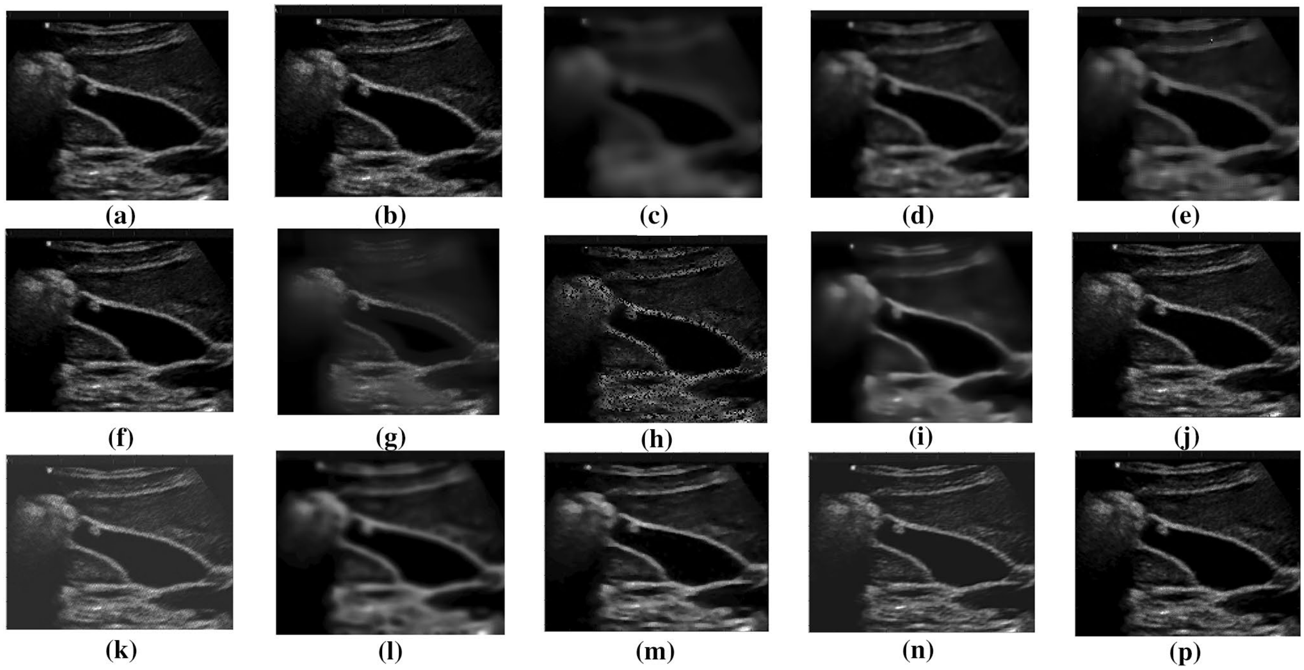

Fig. 11 Denoised image outputs using different filtering algorithms for real ultrasound image of gall bladder2 for the value of σ = 0.10. **a** Original image, **b** noisy image, **c** F-1, **d** F-2, **e** F-3, **f** F-4, **g** F-5, **h** F-6, **i** F-7, **j** F-8, **k** F-9, **l** F-10, **m** F-11, **n** F-12, **p** F-13

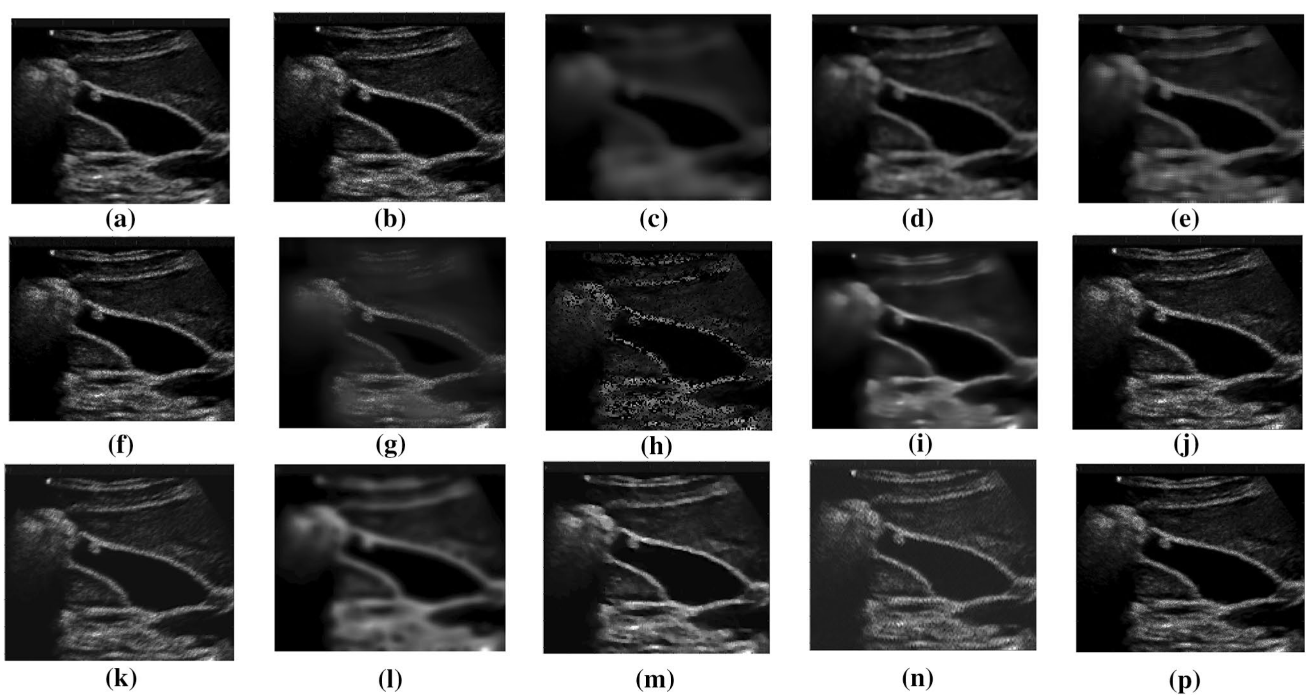

Fig. 12 Denoised image outputs using different filtering algorithms for real ultrasound image of gall bladder2 for the value of σ = 0.20. **a** Original image, **b** noisy image, **c** F-1, **d** F-2, **e** F-3, **f** F-4, **g** F-5, **h** F-6, **i** F-7, **j** F-8, **k** F-9, **l** F-10, **m** F-11, **n** F-12, **p** F-13

despeckling filters and algorithms at 2 different noise levels. From the numerical results, it is observed that for the real clinical ultrasound images the MSE and MAE value of the proposed despeckling filter is significantly low in comparison to other despeckling filters and algorithms. Correspondingly the value of PSNR is comparatively high for the proposed

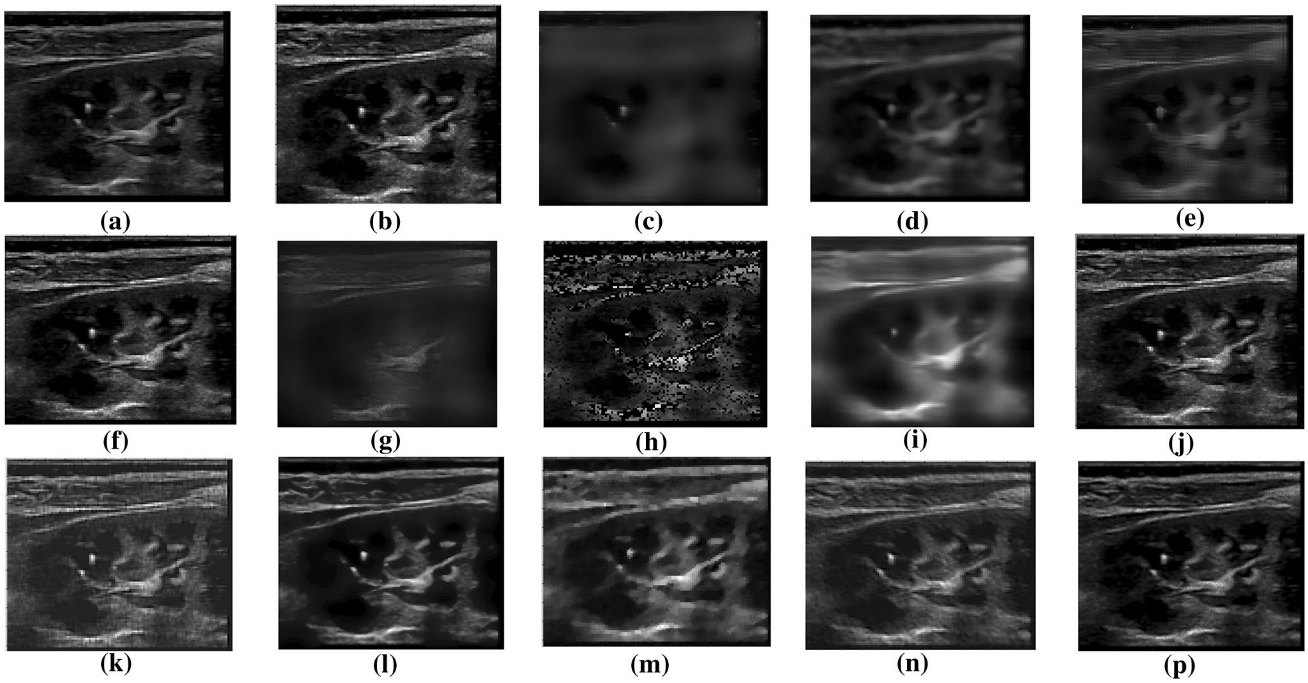

Fig. 13 Denoised image outputs using different filtering algorithms for real ultrasound image of kidney1 for the value of σ = 0.10. **a** Original image, **b** noisy image, **c** F-1, **d** F-2, **e** F-3, **f** F-4, **g** F-5, **h** F-6, **i** F-7, **j** F-8, **k** F-9, **l** F-10, **m** F-11, **n** F-12, **p** F-13

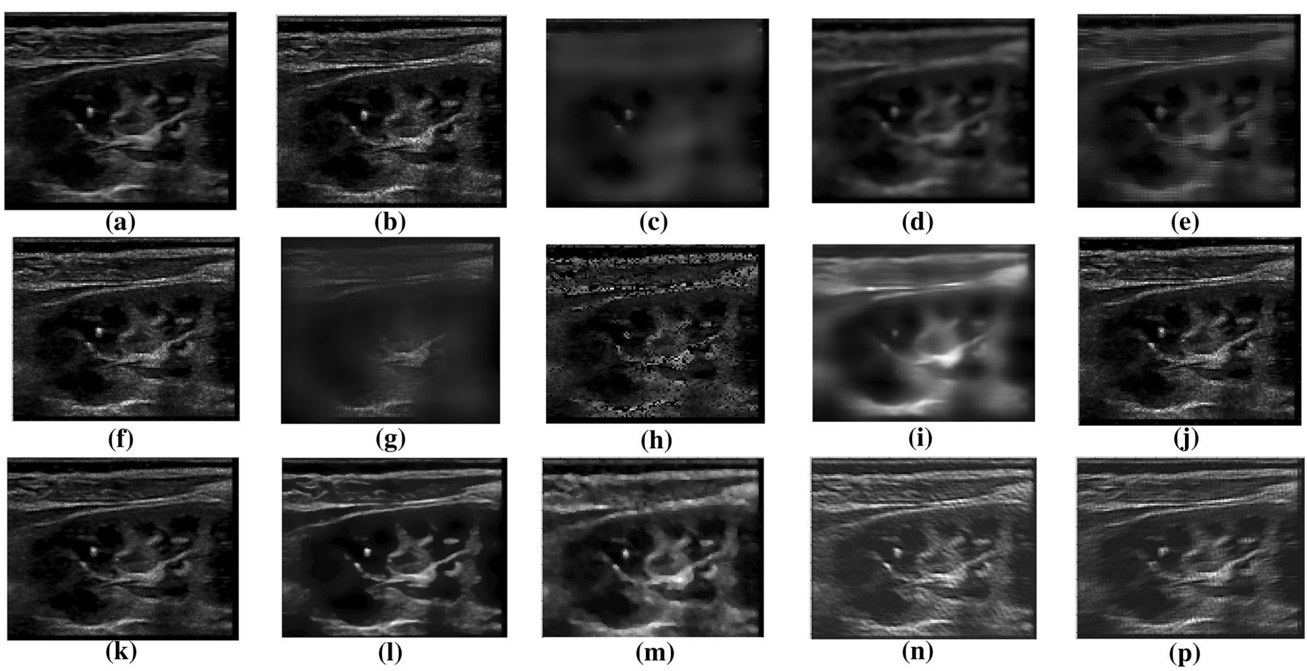

Fig. 14 Denoised image outputs using different filtering algorithms for real ultrasound image of kidney1 for the value of σ = 0.20. **a** Original image, **b** noisy image, **c** F-1, **d** F-2, **e** F-3, **f** F-4, **g** F-5, **h** F-6, **i** F-7, **j** F-8, **k** F-9, **l** F-10, **m** F-11, **n** F-12, **p** F-13

algorithm. From the above discussion, it is clear that the proposed despeckling filter effectively removes the speckle noise from the real clinical ultrasound images and also gives the better visual quality in comparison to other existing despeckling filters. The competitive SSIM value of the proposed filter

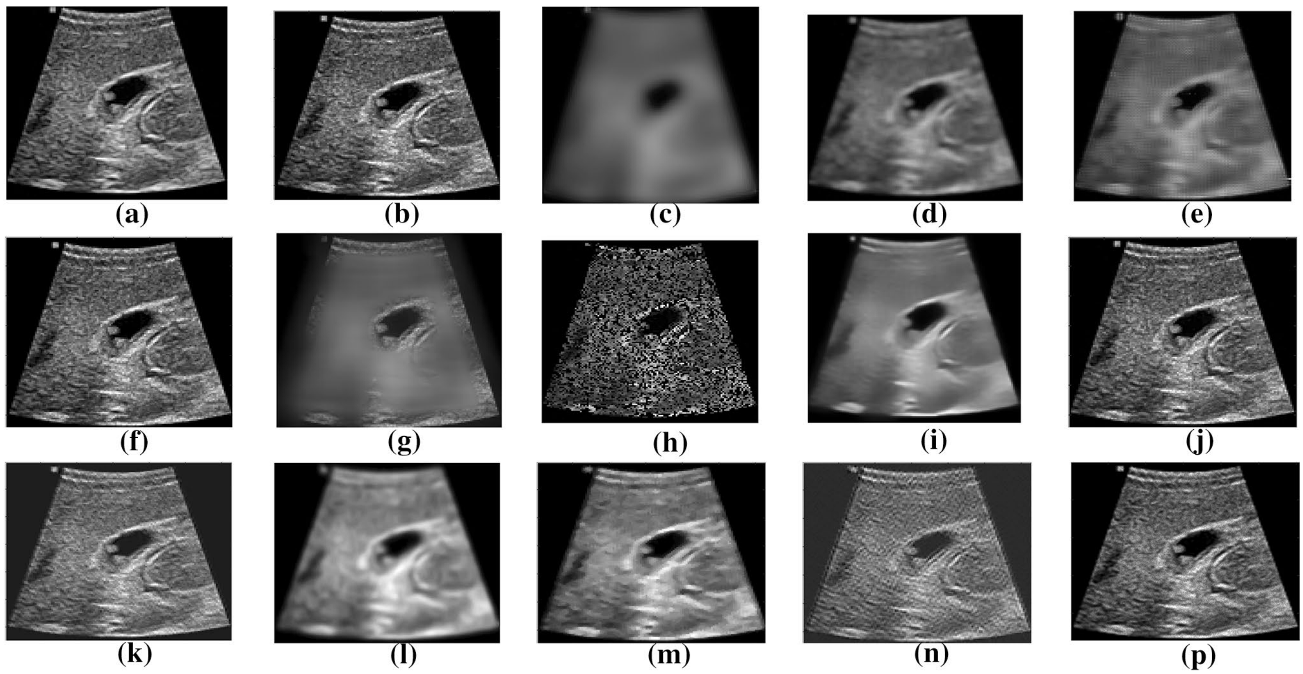

Fig. 15 Denoised image outputs using different filtering algorithms for real ultrasound image of gall bladder3 for the value of σ = 0.10. **a** Original image, **b** noisy image, **c** F-1, **d** F-2, **e** F-3, **f** F-4, **g** F-5, **h** F-6, **i** F-7, **j** F-8, **k** F-9, **l** F-10, **m** F-11, **n** F-12, **p** F-13

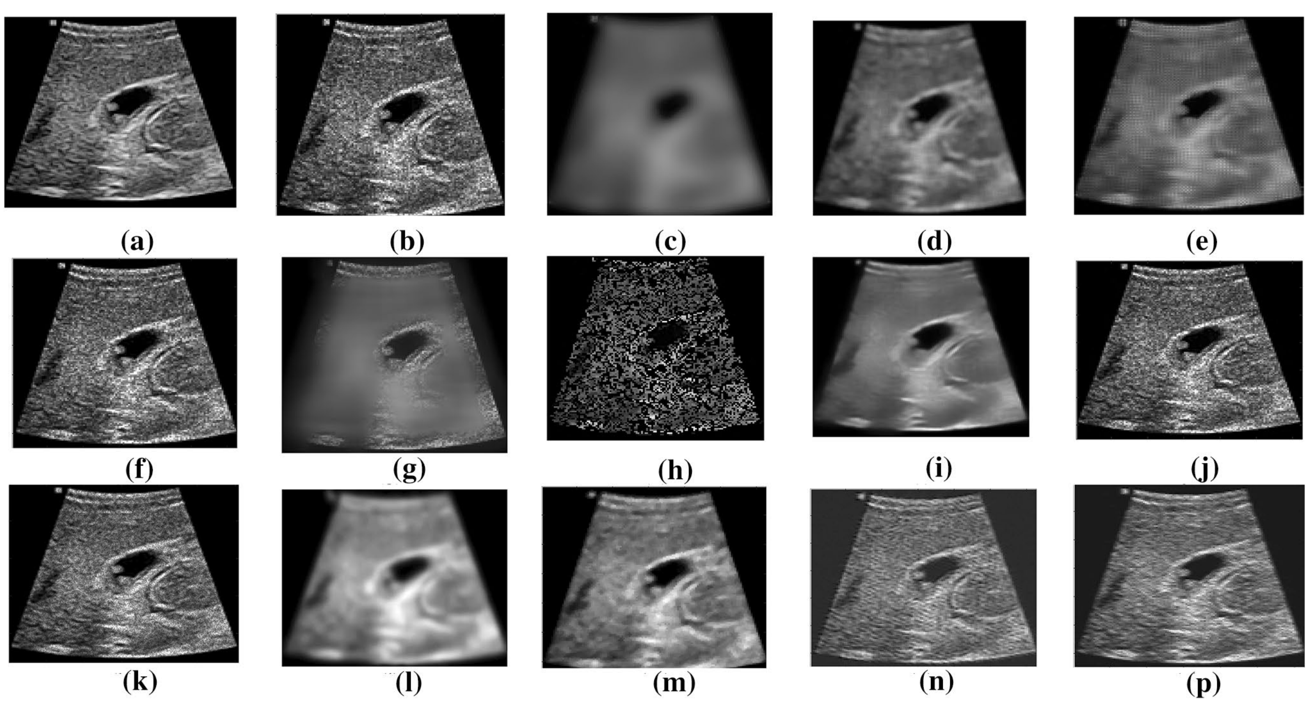

Fig. 16 Denoised image outputs using different filtering algorithms for real ultrasound image of gall bladder3 for the value of σ = 0.20. **a** Original image, **b** noisy image, **c** F-1, **d** F-2, **e** F-3, **f** F-4, **g** F-5, **h** F-6, **i** F-7, **j** F-8, **k** F-9, **l** F-10, **m** F-11, **n** F-12, **p** F-13

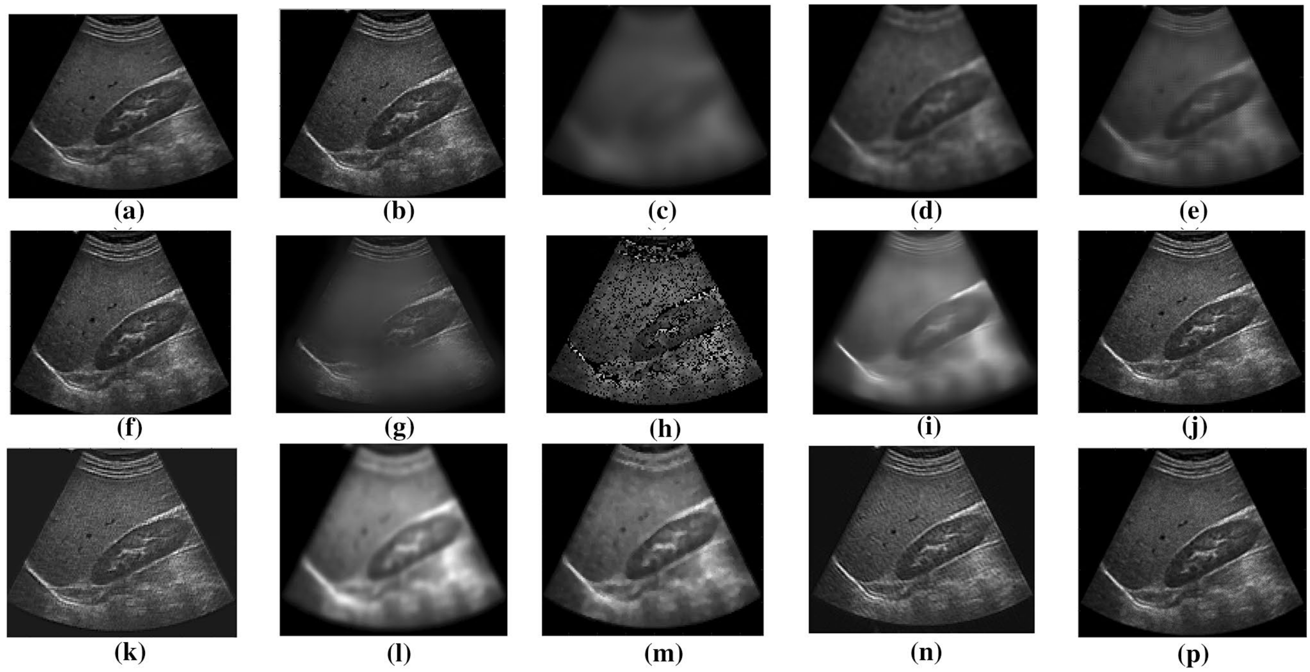

Fig. 17 Denoised image outputs using different filtering algorithms for real ultrasound image of kidney2 for the value of σ = 0.10. **a** Original image, **b** noisy image, **c** F-1, **d** F-2, **e** F-3, **f** F-4, **g** F-5, **h** F-6, **i** F-7, **j** F-8, **k** F-9, **l** F-10, **m** F-11, **n** F-12, **p** F-13

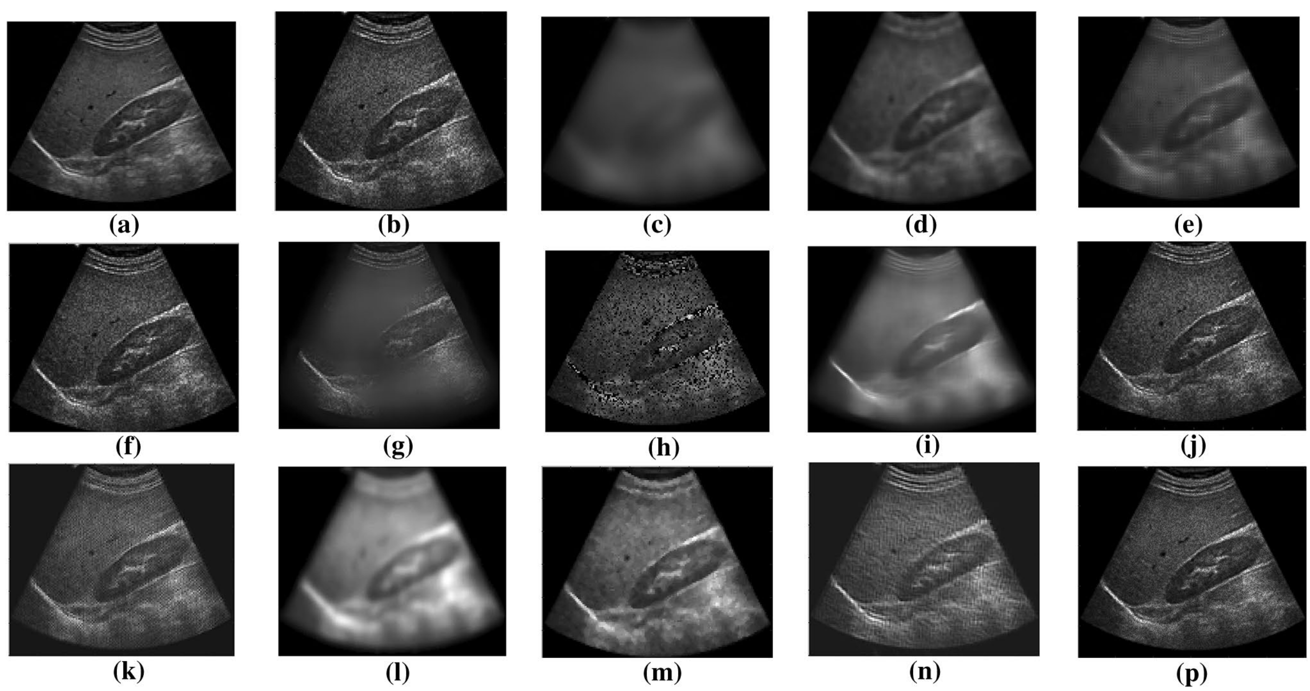

Fig. 18 Denoised image outputs using different filtering algorithms for real ultrasound image of kidney2 for the value of σ = 0.20. **a** Original image, **b** noisy image, **c** F-1, **d** F-2, **e** F-3, **f** F-4, **g** F-5, **h** F-6, **i** F-7, **j** F-8, **k** F-9, **l** F-10, **m** F-11, **n** F-12, **p** F-13

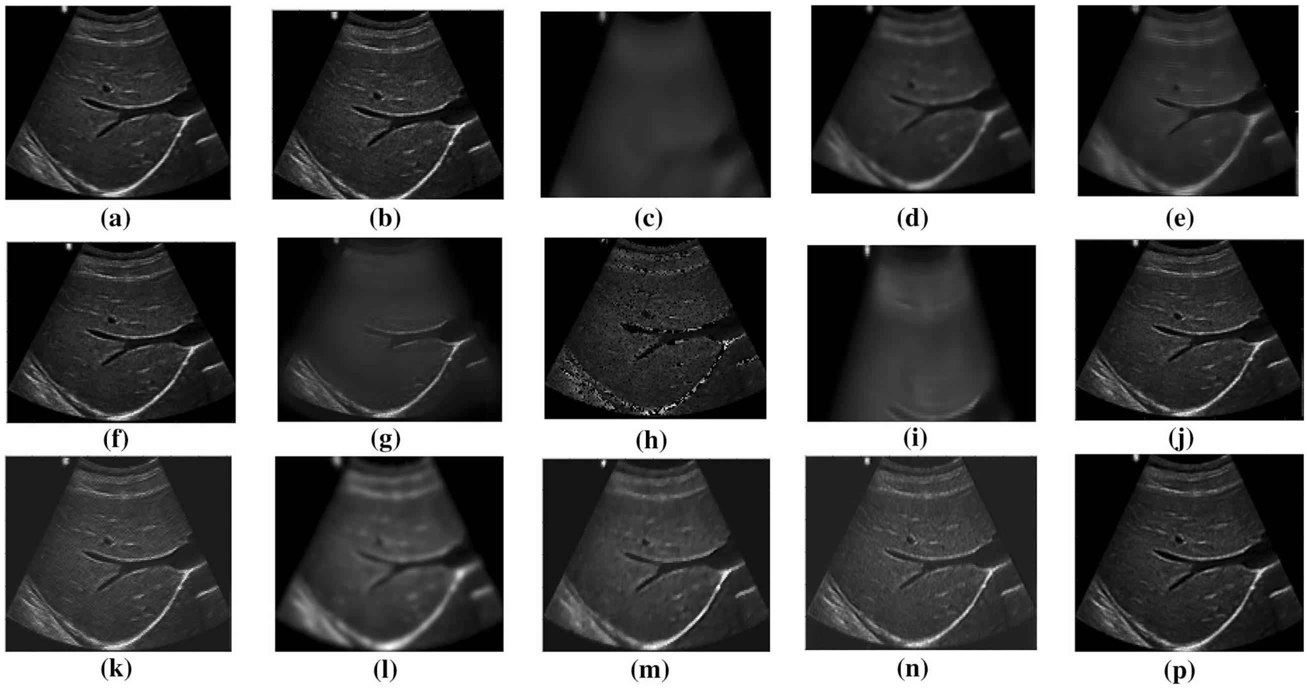

Fig. 19 Denoised image outputs using different filtering algorithms for real ultrasound image of liver1 for the value of σ = 0.10. **a** Original image, **b** noisy image, **c** F-1, **d** F-2, **e** F-3, **f** F-4, **g** F-5, **h** F-6, **i** F-7, **j** F-8, **k** F-9, **l** F-10, **m** F-11, **n** F-12, **p** F-13

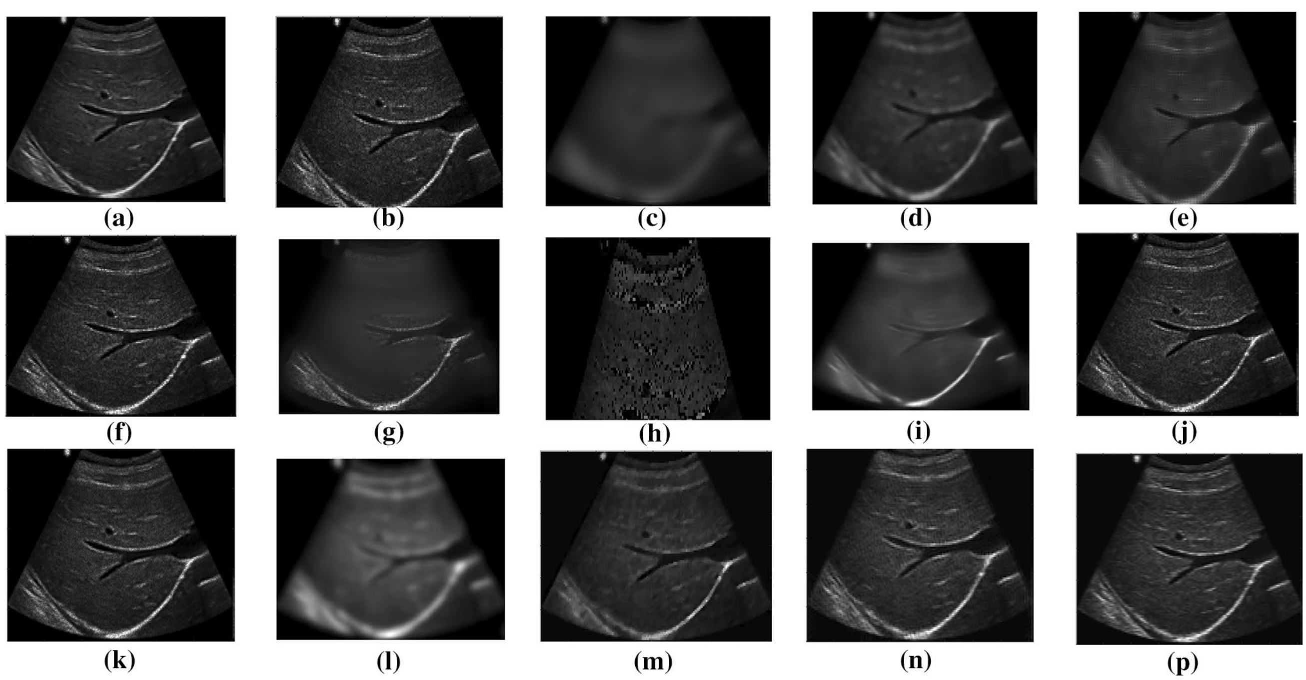

Fig. 20 Denoised image outputs using different filtering algorithms for real ultrasound image of liver1 for the value of σ = 0.20. **a** Original image, **b** noisy image, **c** F-1, **d** F-2, **e** F-3, **f** F-4, **g** F-5, **h** F-6, **i** F-7, **j** F-8, **k** F-9, **l** F-10, **m** F-11, **n** F-12, **p** F-13

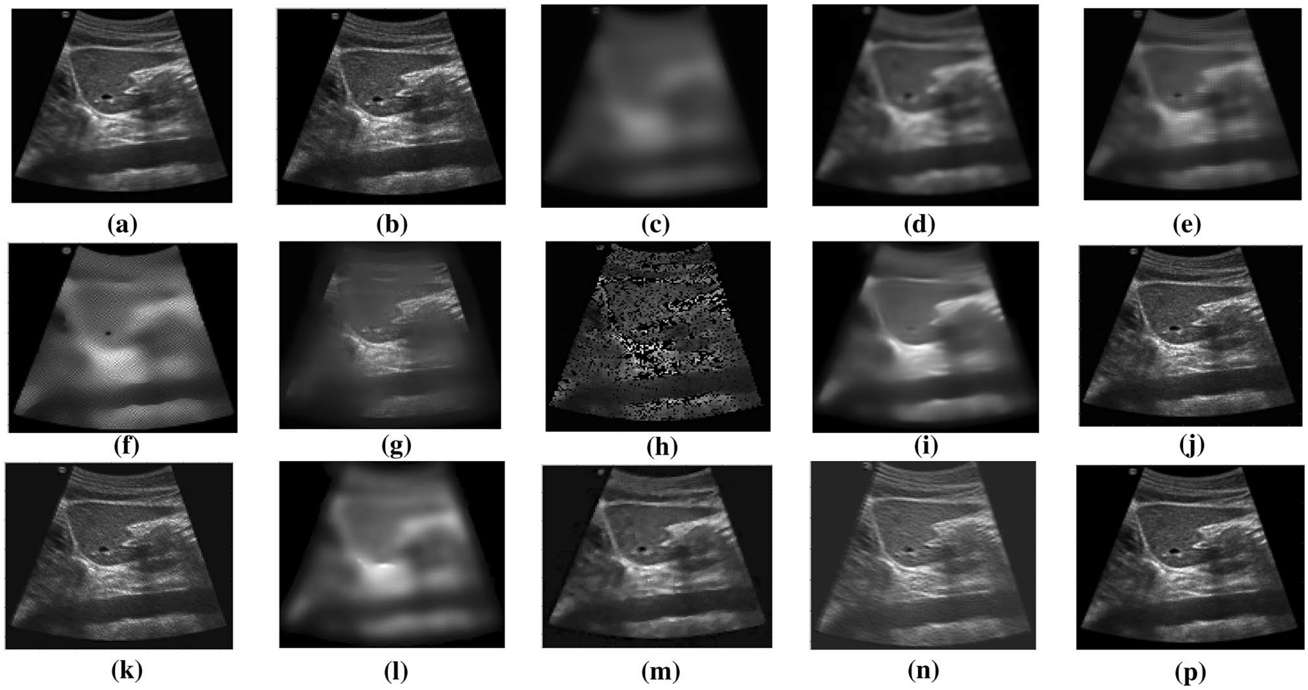

Fig. 21 Denoised image outputs using different filtering algorithms for real ultrasound image of liver2 for the value of σ = 0.10. **a** Original image, **b** noisy image, **c** F-1, **d** F-2, **e** F-3, **f** F-4, **g** F-5, **h** F-6, **i** F-7, **j** F-8, **k** F-9, **l** F-10, **m** F-11, **n** F-12, **p** F-13

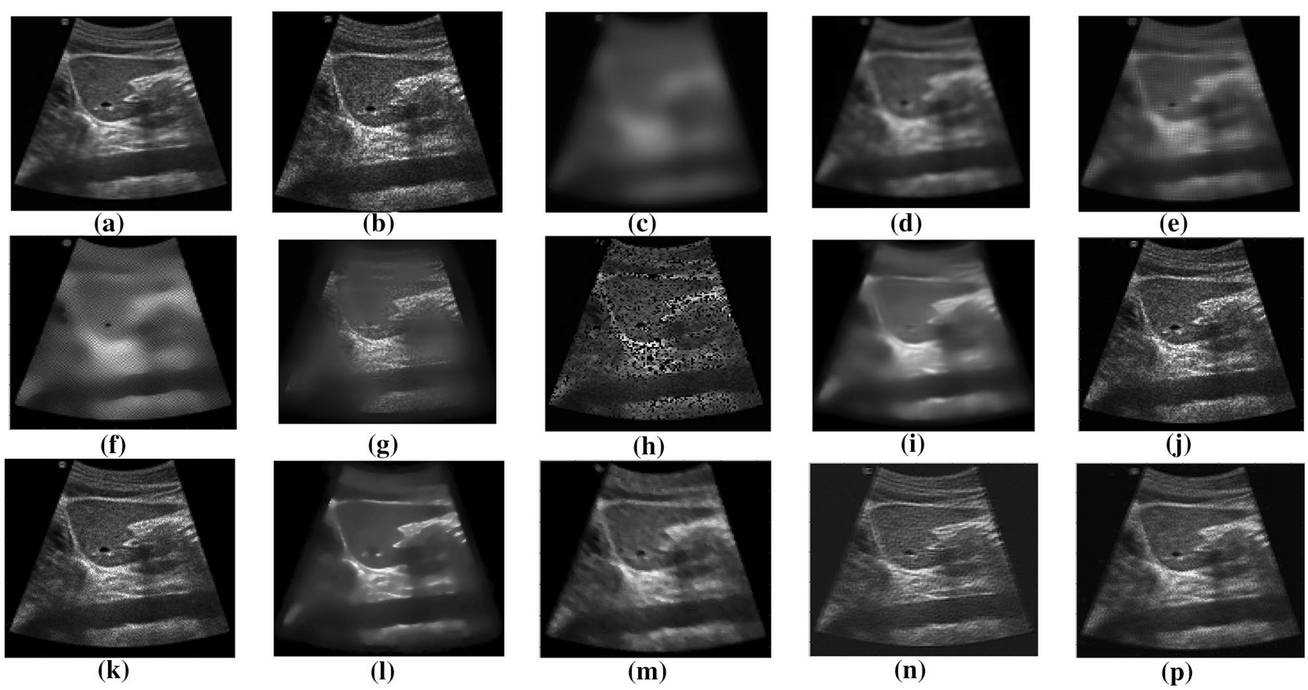

Fig. 22 Denoised image outputs using different filtering algorithms for ultrasound image of liver2 for the value of σ = 0.20. **a** Original image, **b** noisy image, **c** F-1, **d** F-2, **e** F-3, **f** F-4, **g** F-5, **h** F-6, **i** F-7, **j** F-8, **k** F-9, **l** F-10, **m** F-11, **n** F-12, **p** F-13

algorithm is also revealed that the proposed despeckling filter has better edge preserving capability for different noise levels.

Hence, in the light of above results, we can summarize that the proposed despeckling filter preserves and enhance the fine detail of the noisy real ultrasound images that may be required for diagnostic purposes.

6 Conclusion

In this study, we proposed a two dimensional cuckoo search optimization algorithm based despeckling filter for real ultrasound images. In this proposed despeckling filter, we have used fast non-local means filter and 2D FIR filter with Cuckoo's Search algorithm (CSA) to reduce the speckle noise present in the real ultrasound images. This research explored the FNLM filter, 2D FIR filter, and CSA as an optimization tools and studied the denoising effect of different despeckling filters and algorithms on real clinical ultrasound images. The CSA was used to optimize the weight factor of 2D-FIR filter for despeckling the real clinical ultrasound test image. Experiments were conducted for despeckling the real clinical ultrasound images corrupted with multiplicative speckle noise by different noise variance levels (i.e. 0.10 and 0.20). PSNR, MSE, MAE and SSIM numerical values were evaluated to compare the performance of proposed despeckling filter and other existing despeckling filters and algorithms. To make a healthy comparison of proposed despeckling filter with other existing despeckling filters and algorithms, all parameters for different algorithms are same as proposed in the literature by different researchers. The visual and numerical results demonstrated that efficiency of the proposed despeckling filter was better in comparison to other existing despeckling filters and algorithms in preserving significant information of real clinical ultrasound images. The major advantages of our proposed despeckling filter are: (1) computational complexity is less because it does not require any transformation (2) it uses the fixed number of iterations to reach the minimum possible value of MSE. The limitation of our proposed despeckling filter is its objective function as we considered only MSE, other image quality metrics or their combinations could be used to further improve the results. As a future study, the proposed despeckling approach can be extended to other type of images and noise formats as well. The proposed despeckling filter was tested on 2D images, can be extended to 3D images.

References

Achim A, Bezerianos A, Tsakalides P (2001) Novel Bayesian multiscale method for speckle removal in medical ultrasound images. IEEE Trans Med Imaging 20(8):773–783

Atto AM, Pastor D, Mercier G (2009) Smooth adaptation by sigmoid shrinkage. EURASIP J Image Video Process 2009:1–16

Boudjelaba K, Chikouche D, Ros F (2011) Evolutionary techniques for synthesis of 2-D FIR filters. In: IEEE statistical signal processing workshop (SSP), pp 601–604

Buades A, Coll B, Morel JM (2005) A review of image denoising algorithms with a new one. Multiscale Model Simul 4(2):490–530

Coupe P, Yger P, Prima S, Hellier P, Kerveann C, Barillot C (2008) An optimized blockwise non local means denoising filter for 3D magnetic resonance images. IEEE Trans Med Imaging 27(4):425–441

Coupe P, Hellier P, Kervrann C, Barillot C (2009) Nonlocal means-based speckle filtering for ultrasound images. IEEE Trans Image Process 18(10):2221–2229

Cronan JJ (2006) Ultrasound is there a future in diagnostic imaging. J Am Coll Radiol 3(9):645–646

De Paiva JL, Toledo CF, Pedrini H (2016) An approach based on hybrid genetic algorithm applied to image denoising problem. Appl Soft Comput 46:778–791

Dhawan AP (2003) Medical image analysts, Wiley, Hoboken

Frost VS, Stiles JA, Shanmugan KS, Holtzman J (1982) A model for radar images and its application to adaptive digital filtering of multiplicative noise. IEEE Trans Pattern Anal Mach Intell 4(2):157–166

Hacini M, Hachouf F, Djemal K (2014) A new speckle filtering method for ultrasound images based on a weighted multiplicative total variation. J Signal Process 103:214–229

Hao X, Gao S, Gao X (1994) A novel multiscale nonlinear thresholding method for ultrasonic speckle suppressing. IEEE Trans Med Imaging 18:787–794

Hillery D, Chin RT (1991) Iterative Wiener filters for images restorations. IEEE Trans Signal Process 39:1901–1904

Kang J, Lee JY, Yoo Y (2016) A new feature-enhanced speckle reduction method based on multiscale analysis for ultrasound B-mode imaging. IEEE Trans Biomed Eng 63(6):1178–1189

Karaboga N, Getinkaya B (2006) Design of digital FIR filters using differential evolution algorithm. Circuits Syst Signal Process 25(5):649–660

Kaun D, Sawchuck A, Strand T, Chaved P (1985) Adaptive noise smoothing filter for images with signal-dependent noise. IEEE Trans Pattern Anal Mach Intell 7(2):165–177

Kevrann C, Boulanger J (2006) Optimal spatial adaptation for patch based image denoising. IEEE Trans Image Process 15(10):2866–2878

Kockanata S, Karaboga N (2015) A novel 2D-ABC adaptive filter algorithm: a comparative study. J Digit Signal Process 40:140–153

Krissian K, Westin CF, Kikinis R, Vosburgh KG (2007) Oriented speckle reducing anisotropic diffusion. IEEE Trans Image Process 16(5):1412–1424

Latifoglu F (2013) A novel approach to speckle noise filtering based on artificial bee colony algorithm: ultrasound image applications. Comput Methods Progress Biomed 111(3):561–569

Lee JS (1980) Digital image enhancement and noise filtering by use of local statistics. IEEE Trans Pattern Anal Mach Intell 2:165–168

Li ZW, Ding XL, Zheng DW, Hung C (2008) Least squares-based filter for remote sensing image noise reduction. IEEE Trans Geosci Remote Sens 46(7):2044–2049

Loupas T, Mc Dicken W, Allan P (1989) An adaptive weighted median filter for speckle suppression in medical ultrasound images. IEEE Trans Circuits Syst 36(1):129–135

Luong HQ, Ledda A, Philips W (2006) Non-local image interpolation. In: IEEE international conference on image processing, pp 693–696

Malik M, Ahsan F, Mohsin S (2016) Adaptive image denoising using cuckoo algorithm. Soft Comput 20(3):925–938

Mastorakis NE, Gonos F (2003) Design of two-dimensional recursive filters using genetic algorithms. IEEE Trans Circuits Syst Fundam Theory Appl 50(5):634–639

Ogier A, Hellier P, Barillot C (2006) Restoration of 3D medical images with total variation scheme on wavelet domains (TVW). In: Proceedings of the SPIE medical imaging, vol 6144, pp 465–473
Rakhshani H, Rahati A (2016) Snap-drift cuckoo search: a novel cuckoo search optimization algorithm. Appl Soft Comput 52:771–794
Ramos-Llorden G, Vegas-Sánchez-Ferrero G, Martin-Fernandez M (2015) Anisotropic diffusion filter with memory based on speckle statistics for ultrasound images. IEEE Trans Image Process 24(1):345–358
Santiago AF, Carlos AL (2006) On the estimation of coefficient of variation for anisotropic diffusion speckle filtering. IEEE Trans Image Process 15(9):2694–2701
Soni V, Bhandari AK, Kumar A, Singh GK (2013) Improved sub-band adaptive thresholding function for denoising of satellite image based on evolutionary algorithms. IET Signal Proc 7(8):720–730
Suresh S, Lal S (2016) An efficient cuckoo search algorithms based multilevel thresholding for segmentation of satellite images using different objective functions. Expert Syst Appl 58(c):184–209
Szabo TL (2004) Diagnostic ultrasound imaging: inside out (biomedical engineering). Elsevier Academic Press, Amsterdam
Thijssen JM, Obsterveld BJ (1990) Texture in tissue echograms speckle or information? J Ultrasound Med 9(4):215–229
Yang XS, Deb S (2009) Cuckoo search via levy flight. In: IEEE world congress on nature and biologically inspired computing, NaBIC, pp 210–214
Yu Y, Acton ST (2002) Speckle reducing anisotropic diffusion. IEEE Trans Image Process 11(11):1260–1270
Zhang J, Wu L, Lin G, Cheng Y (2017) An integrated de-speckling approach for medical ultrasound images based on wavelet and trilateral filter. Circuits Syst Signal Process 36(1):297–314
Zhou W, Conrad BA, Rahim SH (2004) Image quality assessment: from error visibility to structural similarity. IEEE Trans Image Process 13(4):600–612